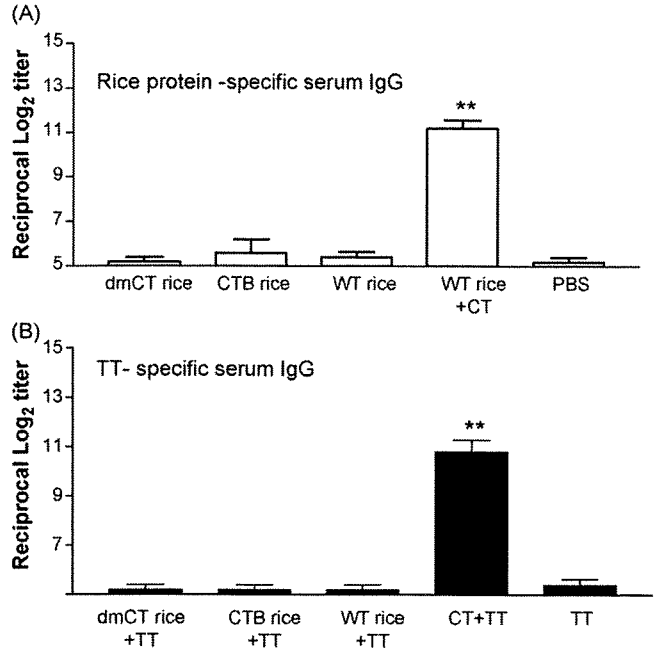

Fig. 3. Lack of adjuvant activity by MucoRice-dmCT. Mice were immunised with rice-expressed dmCT (200 mg power containing 20 μg of dmCTA and 50 μg of CTB), CTB (100 mg power containing 150 μg of CTB), wild-type (WT) rice (200 mg powder), WT rice (200 mg powder) together with 10 μg of CT dissolved in PBS, or PBS alone as a control. Rice-storage-protein-specific IgG responses were not induced in mice immunised with rice-expressed dmCT, CTB, or WT rice or PBS, but they were induced in mice that received WT rice together with CT (A). Mice were immunised with TT (250 μg) alone dissolved in PBS as a control, or the same amount of TT together with rice-expressed dmCT (200 mg power), CTB (100 mg power), WT rice (200 mg powder), or CT (10 μg). TT-specific IgG responses were not induced in mice immunised with TT alone or with TT together with rice-expressed dmCT, CTB, or WT rice. They were induced in mice that received TT together with CT (B).

CTB rice may be related to the presence or absence of the KDEL signal.

3.2. Rice-expressed dmCT induces no rice-protein- or co-administered TT-specific immune responses after oral administration

Because dmCT is known to be an effective mucosal adjuvant when administered nasally, we first examined whether rice-expressed dmCT would induce rice-protein-specific immune responses. Oral administration of MucoRice-dmCT or -CTB did not induce rice-storage protein-specific antibody immune responses (Fig. 3A). This finding suggested that, like MucoRice-CTB, MucoRice-dmCT had no mucosal adjuvant activity. This finding was further confirmed by the results of an oral immunisation study with 250 μg of TT plus either MucoRice-dmCT, MucoRice-CTB or WT rice. None of the co-administered rice preparations supported the generation of TT-specific antibody immune responses (Fig. 3B). In contrast, oral immunisation of a group of mice with TT and CT induced antigen-specific IgG antibody responses to the co-administered protein vaccine antigen (Fig. 3A and B). These findings demonstrated that rice-expressed dmCT (or CTB) showed no adjuvanticity to co-administered TT or to rice protein.

3.3. Rice-expressed dmCT induces CTB- but not CTA-specific immune responses in both systemic and mucosal compartments after oral administration

To examine the oral immunogenicity of MucoRice-dmCT, mice were orally immunised with seed powders prepared from

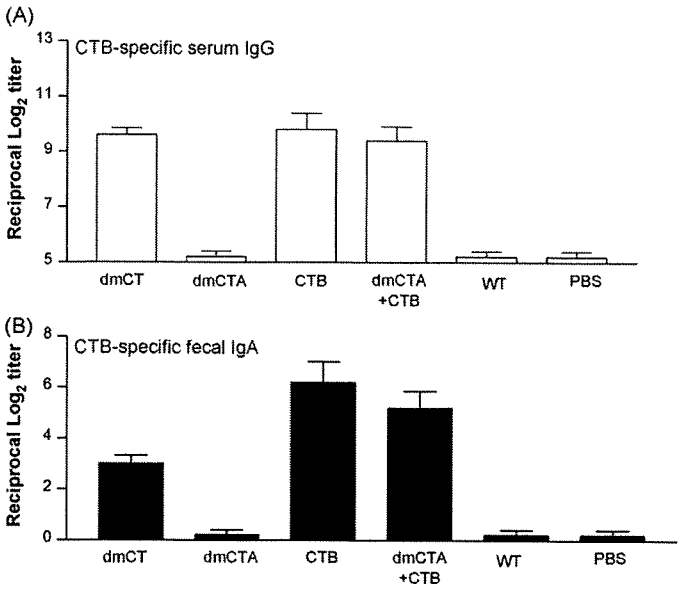

Fig. 4. Induction of CTB-specific antibody responses in mice orally immunised with MucoRice-dmCT. Mice were immunised with rice-expressed dmCT (200 mg power containing 20 μg of dmCTA and 50 μg of CTB), dmCTA (250 mg power containing 12.5 μg of mCTA), CTB (50 mg power containing 75 μg of CT-B), dmCTA (200 mg power containing 10 μg of dmCTA) plus CTB (50 mg power containing 75 μg of CTB), wild-type (WT) rice (200 mg powder) dissolved in PBS, or PBS alone as a control. Equal CTB-specific IgG responses were induced in mice immunised with rice-expressed dmCT, CTB, or dmCT plus CTB, but not in mice that received dmCTA, WT rice, or PBS alone (A). CTB-specific faecal IgA responses were also induced in mice immunised with rice-expressed dmCT, CTB, or dmCT plus CTB, but this mucosal response depended on the dose of CTB (B).

MucoRice expressing dmCT, dmCTA, CTB or dmCTA plus CTB, or from WT rice. CTB-specific serum IgG and mucosal IgA antibodies were detected in mice immunised with 200 mg (20 μg of dmCTA and 50 μg of CTB) of MucoRice-dmCT, 50 mg (75 μg of CTB) of MucoRice-CTB or 200 mg (10 μg of dmCTA) of MucoRice-dmCTA plus 50 mg (75 μg of CTB) of MucoRice-CTB (Fig. 4). The difference between the rice-expressed dmCT and CTB in terms of induction of CTB-specific mucosal IgA antibody response depended on the level of expression of CTB. CTA-specific serum IgG or mucosal IgA antibodies were not detected in mice immunised with seed powders prepared from all transgenic rice lines including 250 mg (12.5 μg of dmCTA) of MucoRice-dmCTA or 200 mg (20 μg of dmCTA) of MucoRice-dmCT (data not shown).

3.4. Rice-expressed dmCT induces protective immunity against CT

To examine the biological activity of CTB-specific antibodies induced by oral administration of MucoRice-dmCT or MucoRice-CTB, CT-neutralising activities were investigated by using a GM1-binding inhibition assay with GM1-ELISA and an elongation assay with CHO cells. As negative controls we used serum antibodies from mice orally immunised with MucoRice-dmCTA or WT rice. Serum samples from mice orally immunised with rice-expressed dmCT, CTB, dmCTA plus CTB or dmCTA or with WT rice or PBS, were subjected to GM1-ELISA. Binding of CT to the coated GM1 ganglioside was blocked in serum samples isolated from mice orally immunised with MucoRice-dmCT, -CTB or -dmCTA plus CTB but not MucoRice-dmCTA or WT rice or PBS (Fig. 5A). Furthermore, elongation assay revealed no morphological changes in CHO cells co-cultured with CT that had been pretreated with serum from mice orally vaccinated with MucoRice-dmCT or -CTB (Fig. 5B). In contrast, CT pretreated with serum from mice immunised with MucoRice-dmCTA or WT rice gave massive elongation of CHO cells

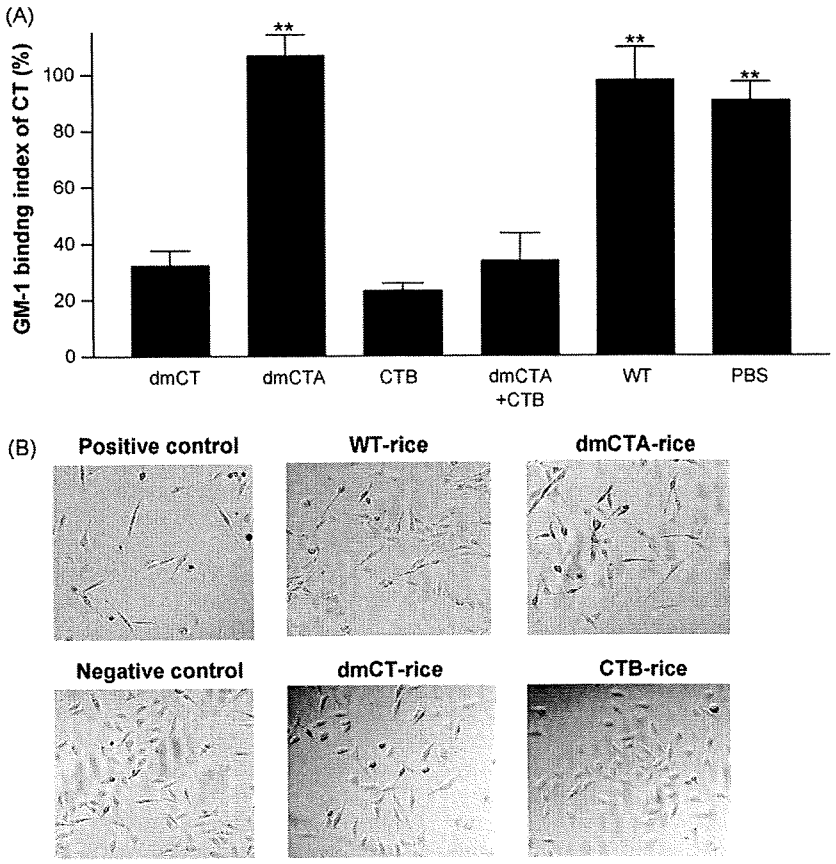

Fig. 5. *In vitro* demonstration of neutralising antibody induction by oral vaccination with MucoRice-dmCT. (A) Neutralising indices, calculated with OD_{450nm} obtained by GM1-ELIZA. Sera of mice immunised with rice-expressed dmCT, CTB, or CTB plus dmCTA, but not with rice-expressed dmCTA, wild-type (WT) rice, or PBS completely blocked the binding of CT to coated GM-1-ganglioside. (B) Elonintesinalgation assay with CHO cells revealed a morphology similar to that of normal cells when the cells were stimulated with CT pretreated with sera from mice immunised with rice-expressed dmCT or CTB. In contrast, there was marked elongation of cells stimulated by CT pretreated with sera from mice immunised with WT rice or rice-expressed dmCTA. Immunisation conditions are as described in Fig. 4.

(Fig. 5B), similar to that induced by the non-pretreated native form of CT. These results revealed that subunit MucoRice-dmCT could induce biologically active antibodies that not only had a GM-1 binding inhibition effect but were also able to neutralise CHO elongation.

Finally, in an *in vivo* CT oral challenge experiment, mice orally vaccinated with powder forms of MucoRice-dmCT, -CTB or -dmCTA plus CTB showed no, to very weak, clinical signs of diarrhoea, whereas those given MucoRice-dmCTA, WT rice or PBS orally developed severe diarrhoea (Fig. 6). The volumes of intestinal fluid in mice immunised with MucoRice-dmCT, -CTB or -dmCTA plus CTB were significantly lower after oral challenge with CT than the volumes in mice given WT rice or demCTA rice or PBS. Interestingly, the reduction in volume of intestinal fluid depended on the level of mucosal CTB-specific IgA antibody but not on that of systemic CTB-specific IgG antibody (Fig. 4). These data demonstrated that

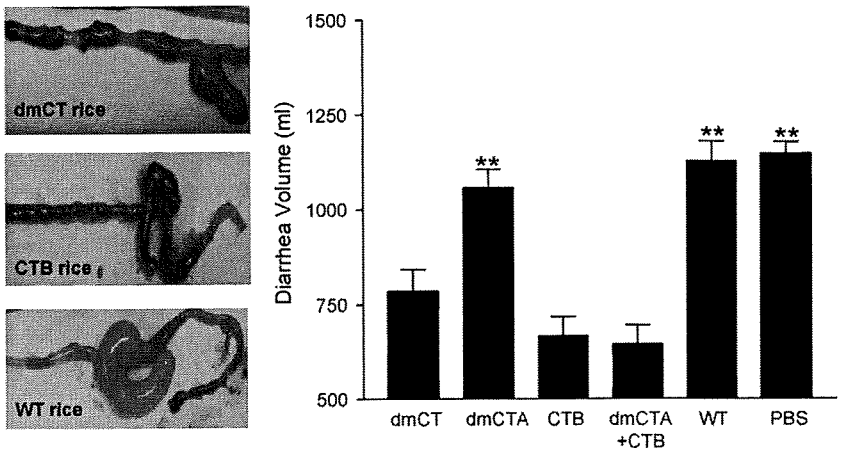

Fig. 6. Induction of protective immunity against CT by oral immunisation with MucoRice-dmCT. Mice immunised with rice-expressed dmCT, CTB, or CTB plus dmCTA, but not with rice-expressed dmCTA, wild-type (WT) rice, or PBS showed no symptoms of diarrhoea and low volumes of intestinal fluid. Immunisation conditions are as described in Fig. 4.

oral vaccination with MucoRice-dmCT could induce a high level of protective antibody response against CT challenge.

4. Discussion

It is well known that oral administration of CT to mice induces strong protective immunity against CT-induced diarrhoea [16]. Although appropriate oral administration of CT itself can protect mice from toxin-induced diarrhoea, it is unsuitable for use in humans because of its toxicity, causing severe diarrhoea if given orally. To overcome this obstacle, a killed *Vibrio cholerae* vaccine combined with recombinant CTB was successfully developed and approved by the European Union in 2004 and in many other regions, including South Asia and South America [17]. Although the killed cholera vaccine has been shown to be useful, further advances are required in the practical aspects of vaccine production and global distribution. For instance, the vaccine is not heat stable; instead, it requires a "cold chain" en route from vaccine manufacture to the field of vaccination [18,19]. In this regard, the rice expression system is recognised as a new form of bioreactor for cost-effective production of large-scale recombinant proteins on an industrial scale and offers a highly practical global strategy for cold-chain and needle-free vaccination against infection [3]. In fact, CTB-expressing transgenic rice seeds (or MucoRice-CTB) preserved for over 1.5 years at room temperature have been shown to induce both systemic and mucosal antigen-specific immune responses for the protection of mice against CT-induced diarrhoea [3]. Our additional and separate data (Tokuhara, D., et al., manuscript in preparation) show that the MucoRice system maintained the immunogenicity of expressed vaccine at room temperature for 2.5 years.

Here, we expressed two major subunits (A and B) of nontoxic mutant CT in a MucoRice system. We used dmCT as an example of nontoxic cholera toxin for rice transgene expression; it has two amino acid substitutions, in the ADP-ribosyltransferase activity centre (E112K) and the carboxyl-terminal KDEL [6]. dmCT lacks ADP-ribosyltransferase activity, has proven unable to move from the Golgi to the endoplasmic reticulum (ER), and does not elicit fluid accumulation in mouse-ligated ileal loops [6]. These results suggest that dmCT is a good and safe candidate for a vaccine against the toxin. To enhance the accumulation of CTB protein in rice, an ER retention signal (KDEL) was fused to the 3′ end of the CTB genes when we originally established rice-expressed CTB or MucoRice-CTB [3]. In this study, not only did we change the KDEL sequence of the carboxyl terminal of dmCT and dmCTA into KDGL, but we also did not add the KDEL sequence to the CTB gene construct (Fig. 1). There is therefore no potential for orally administered dmCTA or CTB to be redirected to the plasma membrane by retrograde transport via the ER and to thus be taken up from the mucosal surface [6]. Removal of the KDEL signal prevents the intracellular trafficking of dmCTA; we consider this prevention to be an important safety issue.

When dmCT was expressed separately as dmCTA and CTB subunits by using different promoters, SDS-PAGE analysis under non-reducing conditions indicated that dmCT formed a CTB pentamer in rice but did not assemble dmCTA and CTB pentamer (Fig. 2C and D). Because dmCTA gave a 26-kDs band (Fig. 2B), the dmCTA was synthesised with a trypsin-sensitive bond that joined the CTA-1 and CTA-2 to make unnicked dmCTA. Authentic cholera toxin gave two CTA bands, CTA (26 kDa) and CTA-1 (20 kDa), under reducing conditions (Fig. 2B), and the band of CTA-1 shifted the complex between CTA and the CTB pentamer under non-reducing conditions, suggesting that there were unnicked and nicked CTs and that the nicked CT could still assemble CTA and CTB pentamer under non-reducing conditions (Fig. 2C, D). Although native purified CT assembles CTA and CTB pentamer, the association of unnicked CT may be easy to break down under non-reducing conditions when compared with that of nicked CT. If this is the case, it is possible that the dmCTA and CTB subunits may assemble as a weak complex in rice seed. The unnatural forms of mdCTA and CTB expression in the rice protein bodies may explain why MucoRice-dmCT possesses oral immunogenicity of not the CTA but the CTB subunit, which is capable of inducing neutralising antibodies against the toxin.

Although dmCT prepared by an *E. coli* expression system is a potent and safe mucosal adjuvant when administered intranasally [6], assembly of CTA and CTB as an intact molecule has been considered important for adjuvant activity. Here, we expressed rice-based dmCT separately as dmCTA and CTB pentamer, which did not assemble together. The separate expression of dmCTA and CTB in the protein body of the rice seed may contribute to the lack of adjuvant activity. Thus, oral immunisation with MucoRice-dmCT did not induce rice-storage-protein-specific immune responses, whereas oral administration of WT rice in the presence of CT (10 μg) induced a rice-storage-protein-specific immune response (Fig. 3A). In addition, oral administration of MucoRice-dmCT did not support the induction of a co-administered TT-specific immune response (Fig. 4B), suggesting that MucoRice-dmCT is a safe vaccine candidate for oral immunisation because it shows no unnecessary adjuvanticity.

When MucoRice-dmCT was administered orally, we found high CTB-specific antibody responses in both the systemic and mucosal compartments (Fig. 4A and B) but no marked CTA-specific antibody responses in either compartment (data not shown). Mucosal CT (10 μg) can induce CTB-specific antibody responses at both systemic and mucosal sites [20]. In our separate study, we found induction of CTA-specific antibody responses at both sites following oral immunisation of CT (Tokuhara, D., et al., manuscript in preparation). Because MucoRice-dmCT did not assemble an intact form of dmCTA and CTB, its oral administration may be unable to induce CTA-specific immune responses. In support of this view, when the mixture of MucoRice-dmCTA and -CTB was tested, CTB- but not CTA-specific antibody responses were induced (Fig. 4). As an alternative possibility, the removal of ADP-ribosyltransferase activity from CTA may contribute to the lack, or reduction, of A-subunit-specific responses. In this case, the 10–20 μg of dmCTA used for oral immunisation may be too small an amount to induce A-subunit-specific responses. It has been shown that mutant forms of CT with loss of ADP-ribosyltransferase activity, such as mCT and dmCT, maintain their adjuvant activity but have lower immunoenhancing potency than that of the native form of the toxin [6,21]. In support of this possibility, the adjuvanticity of CTA-DD, a chimeric adjuvant CTA with a dimer of an immunoglobulin (Ig)-binding fragment of *Staphylococcus aureus* protein A, has been reported to be dependent on ADP-ribosyltransferase activity [15].

To test the quality of the CTB-specific antibody induced by oral vaccination with MucoRice-dmCT, we used both *in vitro* (e.g., GM1-ELISA and CHO-cell elongation assay) and *in vivo* (e.g., CT oral challenge model) neutralising analyses. The results obtained by the neutralising investigation showed that there were no differences in the quality of the CTB-specific antibody responses among mice orally immunised with MucoRice-dmCT, -CTB, or -dmCTA plus CTB (Figs. 5 and 6). Thus, all of the serum samples from the immunised mice showed similar levels of toxin neutralising activity. Importantly, the reduction in the volume of intestinal fluids caused by oral CT challenge depended on the level of CTB-specific mucosal IgA antibodies but not systemic IgG antibodies (Figs. 4 and 6). A reduction in the volume of CT-induced intestinal fluid was always associated with the presence of antigen-specific mucosal IgA antibodies. Our findings further suggest that effective induction of the production of CTB-specific mucosal SIgA antibodies is crucial for preventing the diarrhoea induced by CT. Together

with our previous findings concerning the rice-based CTB oral vaccine (MucoRice-CTB) [8], our current results demonstrate that subunit MucoRice-dmCT has almost the same protective effect as MucoRice-CTB against CT.

In summary, we successfully developed MucoRice expressing two major components, dmCTA and CTB, and we demonstrated that oral vaccination with MucoRice-dmCT induced protective immunity against CT *in vivo*. MucoRice-dmCT vaccine specifically induced CTB- but not CTA-specific serum IgG and mucosal IgA antibodies. Furthermore, it did not induce rice-protein- or co-administered unrelated antigen-specific immune responses when administered orally. These results showed that MucoRice-dmCT had neither adjuvanticity nor oral immunogenicity of CTA. Taken together, our results show that MucoRice can be used as a multicomponent vaccine expression system. Furthermore, because the quality of the protective immunity induced by MucoRice-dmCT against CT was almost the same of that induced by MucoRice-CTB, MucoRice-dmCT could be used as an experimental tool for analyses of other CT-derivative-based rice vaccines.

Acknowledgments

We thank Nippon Paper Group Inc. and Rohto Pharmaceutical Co. Ltd. for their contribution to the MucoRice development project. This work was supported by the Research and Development Program for New Bio-industry Initiatives of the Bio-oriented Technology Research Advancement Institution (Y.Y.); a Research Fellowship from the Japan Society for the Promotion of Science (T.N.); a Grant-in-Aid from the Ministry of Education, Culture, Sports, Science and Technology (MEXT) and the Ministry and Health and Labour of Japan; funds for the Development of Fundamental Technologies for Production of High-value Materials using Transgenic Plants, from the Ministry of Economy, Trade and Industry; the global COE Program "Center of Education and Research for the Advanced Genome-based Medicine for Personalized Medicine and the Control of Worldwide Infectious Diseases" and an "Academic Frontier" Project for Private Universities matching-fund subsidy from MEXT (to H.K.); funds for Function Analysis of Genes Relevant to Agriculturally Important Traits in the Rice Genome, from the Ministry of Agriculture, Forestry and Fisheries (to F.T.); and NIH grants DE12242 and AG025873 (to K.F.).

References

[1] Streatfield SJ, Jilka JM, Hood EE, Turner DD, Bailey MR, Mayor JM, et al. Plant-based vaccines: unique advantages. Vaccine 2001;19(17–19):2742–8.
[2] Streatfield SJ, Howard JA. Plant-based vaccines. Int J Parasitol 2003;33(5–6):479–93.
[3] Nochi T, Takagi H, Yuki Y, Yang L, Masumura T, Mejima M, et al. Rice-based mucosal vaccine as a global strategy for cold-chain- and needle-free vaccination. Proc Natl Acad Sci USA 2007;104(26):10986–91.
[4] Takagi H, Hiroi T, Yang L, Tada Y, Yuki Y, Takamura K, et al. A rice-based edible vaccine expressing multiple T cell epitopes induces oral tolerance for inhibition of Th2-mediated IgE responses. Proc Natl Acad Sci USA 2005;102(48):17525–30.
[5] Yamamoto S, Takeda Y, Yamamoto M, Kurazono H, Imaoka K, Fujihashi K, et al. Mutants in the ADP-ribosyltransferase cleft of cholera toxin lack diarrheagenicity but retain adjuvanticity. J Exp Med 1997;185(7):1203–10.
[6] Hagiwara Y, Kawamura YI, Kataoka K, Rahima B, Jackson RJ, Komase K, et al. A second generation of double mutant cholera toxin adjuvants: enhanced immunity without intracellular trafficking. J Immunol 2006;177(5):3045–54.
[7] Mekalanos JJ, Swartz DJ, Pearson GD, Harford N, Groyne F, de Wilde M. Cholera toxin genes: nucleotide sequence, deletion analysis and vaccine development. Nature 1983;306(5943):551–7.
[8] Qu le Q, Takaiwa F. Evaluation of tissue specificity and expression strength of rice seed component gene promoters in transgenic rice. Plant Biotechnol J 2004;2(2):113–25.
[9] Goto F, Yoshihara T, Shigemoto N, Toki S, Takaiwa F. Iron fortification of rice seed by the soybean ferritin gene. Nat Biotechnol 1999;17(3):282–6.
[10] Hiei Y, Ohta S, Komari T, Kumashiro T. Efficient transformation of rice (*Oryza sativa* L.) mediated by *Agrobacterium* and sequence analysis of the boundaries of the T-DNA. Plant J 1994;6(2):271–82.
[11] Yuki Y, Byun Y, Fujita M, Izutani W, Suzuki T, Udaka S, et al. Production of a recombinant hybrid molecule of cholera toxin-B-subunit and proteolipid–protein–peptide for the treatment of experimental encephalomyelitis. Biotechnol Bioeng 2001;74(1):62–9.
[12] Kweon MN, Yamamoto M, Watanabe F, Tamura S, Van Ginkel FW, Miyauchi A, et al. A nontoxic chimeric enterotoxin adjuvant induces protective immunity in both mucosal and systemic compartments with reduced IgE antibodies. J Infect Dis 2002;186(9):1261–9.
[13] Arakawa T, Yu J, Chong DK, Hough J, Engen PC, Langridge WH. A plant-based cholera toxin B subunit-insulin fusion protein protects against the development of autoimmune diabetes. Nat Biotechnol 1998;16(10):934–8.
[14] Kothary MH, Claverie EF, Miliotis MD, Madden JM, Richardson SH. Purification and characterization of a Chinese hamster ovary cell elongation factor of *Vibrio hollisae*. Infect Immun 1995;63(7):2418–23.
[15] Agren LC, Ekman L, Lowenadler B, Nedrud JG, Lycke NY. Adjuvanticity of the cholera toxin A1-based gene fusion protein, CTA1-DD, is critically dependent on the ADP-ribosyltransferase and Ig-binding activity. J Immunol 1999;162(4):2432–40.
[16] Lycke N, Erlandsson L, Ekman L, Schon K, Leanderson T. Lack of J chain inhibits the transport of gut IgA and abrogates the development of intestinal antitoxic protection. J Immunol 1999;163(2):913–9.
[17] Hill DR, Ford L, Lalloo DG. Oral cholera vaccines: use in clinical practice. Lancet Infect Dis 2006;6(6):361–73.
[18] Giudice EL, Campbell JD. Needle-free vaccine delivery. Adv Drug Deliv Rev 2006;58(1):68–89.
[19] Varmus H, Klausner R, Zerhouni E, Acharya T, Daar AS, Singer PA. Public health. Grand challenges in global health. Science 2003;302(5644):398–9.
[20] Marinaro M, Staats HF, Hiroi T, Jackson RJ, Coste M, Boyaka PN, et al. Mucosal adjuvant effect of cholera toxin in mice results from induction of T helper 2 (Th2) cells and IL-4. J Immunol 1995;155(10):4621–9.
[21] Yamamoto S, Kiyono H, Yamamoto M, Imaoka K, Fujihashi K, Van Ginkel FW, et al. A nontoxic mutant of cholera toxin elicits Th2-type responses for enhanced mucosal immunity. Proc Natl Acad Sci USA 1997;94(10):5267–72.

LETTERS

Uptake through glycoprotein 2 of FimH$^+$ bacteria by M cells initiates mucosal immune response

Koji Hase[1]*, Kazuya Kawano[1]*, Tomonori Nochi[2], Gemilson Soares Pontes[2], Shinji Fukuda[1,3], Masashi Ebisawa[1,3], Kazunori Kadokura[1,3], Toru Tobe[4], Yumiko Fujimura[1], Sayaka Kawano[1], Atsuko Yabashi[5], Satoshi Waguri[5], Gaku Nakato[1,3], Shunsuke Kimura[1], Takaya Murakami[1], Mitsutoshi Iimura[6], Kimiyo Hamura[6], Shin-Ichi Fukuoka[7], Anson W. Lowe[8], Kikuji Itoh[9], Hiroshi Kiyono[2] & Hiroshi Ohno[1,3]

The mucosal immune system forms the largest part of the entire immune system, containing about three-quarters of all lymphocytes and producing grams of secretory IgA daily to protect the mucosal surface from pathogens[1–3]. To evoke the mucosal immune response, antigens on the mucosal surface must be transported across the epithelial barrier into organized lymphoid structures such as Peyer's patches[4]. This function, called antigen transcytosis, is mediated by specialized epithelial M cells[5,6]. The molecular mechanisms promoting this antigen uptake, however, are largely unknown. Here we report that glycoprotein 2 (GP2), specifically expressed on the apical plasma membrane of M cells among enterocytes, serves as a transcytotic receptor for mucosal antigens. Recombinant GP2 protein selectively bound a subset of commensal and pathogenic enterobacteria, including *Escherichia coli* and *Salmonella enterica* serovar Typhimurium (*S.* Typhimurium), by recognizing FimH, a component of type I pili on the bacterial outer membrane. Consistently, these bacteria were colocalized with endogenous GP2 on the apical plasma membrane as well as in cytoplasmic vesicles in M cells. Moreover, deficiency of bacterial FimH or host GP2 led to defects in transcytosis of type-I-piliated bacteria through M cells, resulting in an attenuation of antigen-specific immune responses in Peyer's patches. GP2 is therefore a previously unrecognized transcytotic receptor on M cells for type-I-piliated bacteria and is a prerequisite for the mucosal immune response to these bacteria. Given that M cells are considered a promising target for oral vaccination against various infectious diseases[7,8], the GP2-dependent transcytotic pathway could provide a new target for the development of M-cell-targeted mucosal vaccines.

M cells are atypical epithelial cells that actively phagocytose macromolecules and microbes. Unlike dendritic cells (DCs) and macrophages, which target antigens to lysosomes for degradation, M cells mainly transcytose the internalized antigens[6]. This vigorous macromolecular transcytosis through M cells delivers antigen to the underlying organized lymphoid follicles and is believed to be essential for initiating antigen-specific mucosal immune responses[9]. Previous studies of mucosal immunity have focused mainly on the roles of mucosal DCs and T lymphocytes, with far less attention on M cells. For example, it is unknown whether antigen transcytosis by M cells is non-specific or mediated by specific receptors that bind to antigens with certain molecular patterns[10]. Efficient transport of luminal microorganisms by M cells led us to speculate that M cells may express transcytotic receptors for particular microorganisms on their apical surface. To identify such receptors we took advantage of a microarray-based approach for a genome-wide survey of M-cell-specific molecules[11,12]. One such molecule, GP2, was previously thought to be expressed exclusively by pancreatic acinar cells of most mammals[13], but our microarray analysis showed that *Gp2* mRNA is also highly expressed in follicle-associated epithelium (FAE) of mouse Peyer's patches, in contrast with intestinal villus epithelium[11]. GP2 expression in FAE was also confirmed by quantitative polymerase chain reaction (qPCR) (Fig. 1a) and immunoblot analyses (Fig. 1b). Data from *in situ* hybridization (Fig. 1c, left) and immunostaining (Fig. 1d) demonstrated that GP2 expression was restricted to M cells in FAE, as depicted by co-staining with an M-cell-recognizing lectin, *Ulex europaeus* agglutinin-1 (UEA-1) (Supplementary Fig. 2; note that UEA-1 also stains goblet cells as indicated by the arrowhead). Apart from M cells from Peyer's patches, GP2 was also widely distributed on M cells in other organized mucosal lymphoid tissues, namely isolated lymphoid follicles, caecal patches and colonic patches, in mice (Fig. 1e). GP2 was also expressed on M cells of human Peyer's patches, as depicted by a similar expression pattern to that of a human M-cell marker, clusterin[14] (Fig. 1c, f, and Supplementary Fig. 3). These observations define GP2 as the first universal M-cell marker in mouse and human.

We next assessed subcellular localization of GP2 in M cells by immunoelectron microscopy. Positive signals for GP2 were localized intensely on the M-cell apical surface (Fig. 1g and Supplementary Fig. 4). This was further confirmed by apical GP2 staining when membranes were not permeabilized (Fig. 1h). GP2 was also detected in the subapical tubulovesicular compartment, most probably endosomes (Fig. 1g, arrowheads), raising the possibility that GP2 could function as an endocytic receptor. To evaluate this possibility, we injected anti-GP2 monoclonal antibody (mAb) into a ligated intestinal loop containing Peyer's patches. Some of the injected mAb remained on the apical plasma membrane of the M cells, but it was also internalized into cytoplasmic vesicular structures (Supplementary Movie 1), supporting a potential function of GP2 on M cells as an endocytic receptor for luminal antigens.

We next sought to identify the luminal antigens bound to GP2. GP2 has a similar domain structure and 52% overall amino acid sequence identity to Tamm–Horsfall protein (THP), which is expressed on the apical plasma membrane of renal tubular epithelium[15]. THP specifically

[1]Laboratory for Epithelial Immunobiology, Research Center for Allergy and Immunology, RIKEN, Kanagawa 230-0045, Japan. [2]Department of Microbiology and Immunology, The Institute of Medical Science, The University of Tokyo, Tokyo 108-8639, Japan. [3]Supramolecular Biology, International Graduate School of Bionanoscience, Yokohama City University, Kanagawa 230-0045, Japan. [4]Graduate School of Medicine, Osaka University, 565-0871 Suita, Osaka, Japan. [5]Department of Anatomy and Histology, Fukushima Medical University, School of Medicine, Fukushima 960-1295, Japan. [6]Institute of Gastroenterology, Tokyo Women's Medical University, Tokyo 162-8666, Japan. [7]Department of Chemistry and Biological Science, College of Science and Engineering, Aoyama Gakuin University, Kanagawa, 229-8558, Japan. [8]Department of Medicine and the Digestive Disease Center, Stanford University, Stanford, California 94305, USA. [9]Veterinary Public Health, Graduate School of Agricultural and Life Sciences, The University of Tokyo, Tokyo 113-8657, Japan.
*These authors contributed equally to this work.

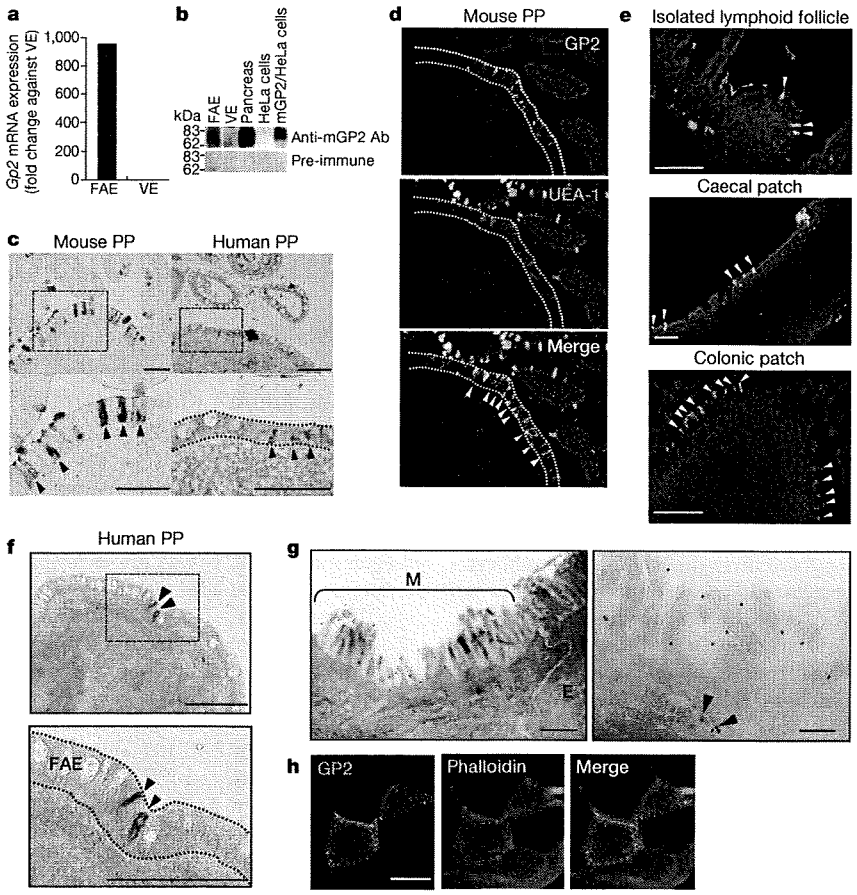

Figure 1 | In the intestine, GP2 is exclusively expressed by mouse and human M cells. **a**, qPCR analysis for mouse *Gp2* mRNA. VE, villus epithelium. **b**, Immunoblotting of mouse GP2 in FAE and villus epithelium. Pancreas and HeLa cells, with or without ectopic expression of a mouse GP2 complementary DNA, are shown as positive controls. Ab, antibody. **c**, *In situ* hybridization analysis using a specific probe for *Gp2* mRNA (purple) in mouse and human Peyer's patch (PP). M cells are co-stained with UEA-1 lectin (brown) in mouse Peyer's patch. Lower panels are magnified images of the areas surrounded by a dotted square in the upper panels. **d**, **e**, Tissue sections prepared from mouse Peyer's patch (**d**) and from isolated lymphoid follicle, caecal patch and colonic patch (**e**) were stained with anti-mouse GP2 mAb (green), UEA-1 (red) and 4,6-diamidino-2-phenylindole (blue). Dotted lines indicate the location of the FAE in the Peyer's patch. GP2-expressing cells scattered in the FAE are indicated by arrowheads. **f**, Immunohistochemical staining of a tissue section of human Peyer's patch with anti-human GP2 mAb. The positive signal appears brown. The blue colour shows counterstaining with haematoxylin. Dotted lines in the lower panel indicate the location of the FAE in human Peyer's patch. **g**, Subcellular localization of GP2 analysed by immunoelectron microscopy. The M cell (indicated by M) is characterized by sparse and irregular microvilli instead of the rigid and closely packed microvilli observed in normal absorptive enterocytes (indicated by E). GP2 expression (indicated by colloidal gold particles) is visible on the apical plasma membrane and also in the subapical tubulovesicular structures (arrowheads). Scale bars, 100 μm (**c**–**f**), 0.5 μm (**g**, left), 0.2 μm (**g**, right). **h**, The luminal side of whole-mount specimens of a Peyer's patch was treated with anti-GP2 mAb and subsequently with Alexa594-labelled secondary antibody (red) without membrane permeabilization, and then counterstained with phalloidin (green) with membrane permeabilization by 0.1% Triton X-100 in PBS. Scale bar, 10 μm.

binds to uropathogenic *E. coli* and promotes bacterial clearance[16]. We therefore reasoned that GP2 might also bind particular enterobacteria. Indeed, fusion proteins of the Fc fragment of human immunoglobulin G1 with mouse and human GP2 (mGP2-Fc and hGP2-Fc, respectively) both bound *E. coli* (Fig. 2a). The binding of GP2 to *E. coli* is largely mediated by FimH present on the type I pilus tip, because deficiency of FimH abrogated the binding (Fig. 2b). FimH is well documented to bind certain glycoproteins specifically in a mannose-dependent fashion[17]. Consistently, the presence of mannose inhibited the interaction between GP2 and *E. coli* (Supplementary Fig. 5). In sharp contrast to the case in *FimH* deletion, the binding was unaffected in the absence of *CsgA* or *FliC*, which encode the main structural component of curli and flagella, respectively. Lipopolysaccharide and peptidoglycan, non-filamentous components of the bacterial outer membrane, did not bind to GP2 (Supplementary Fig. 6). Thus the $FimH^+$ type I pilus binds GP2, which is consistent with a recent study[18]. This view is also supported by our observation that GP2 specifically bound $FimH^+$ (*E. coli*, *S. enterica* serovar Enteritidis and *S.* Typhimurium) bacteria[19] but not $FimH^-$ (*Pseudomonas aeruginosa*, *Listeria monocytogenes* and *Yersinia enterocolitica*) bacteria (Fig. 2c).

The interaction of GP2 with FimH suggested a possible role of GP2 as a transcytotic receptor for type-I-piliated bacteria. We examined this possibility by the ligated intestinal loop assay using *E. coli* expressing green fluorescent protein (GFP). Three-dimensional imaging analysis of M cells with deconvolution microscopy[20,21] demonstrated the accumulation of GP2 around GFP-*E. coli* just being internalized into M cells through the apical plasma membrane (Fig. 2d, e, and Supplementary Movie 2). Similarly, GP2 was colocalized with GFP-expressing *S.* Typhimurium on the apical surface as well as in subapical vesicular structures (Supplementary Fig. 7 and Movie 3). The number of *FimH*-deficient mutants internalized into M cells was significantly lower than that of the wild-type strain (Supplementary Fig. 8). Furthermore, the uptake of type-I-piliated bacteria by M cells was markedly lower in GP2-deficient ($Gp2^{-/-}$) mice than in wild-type ($Gp2^{+/+}$) mice (Supplementary Fig. 9 and Fig. 3a, left). In contrast, there was no significant difference in translocation of

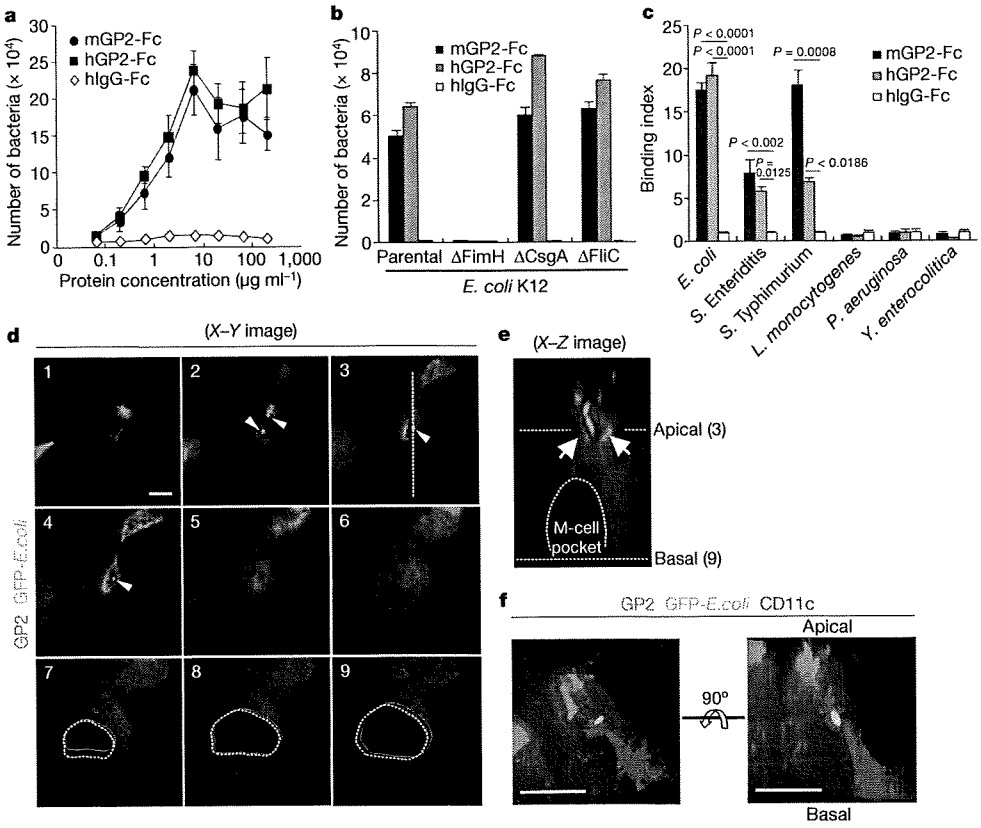

Figure 2 | GP2 binds to FimH-expressing Gram-negative bacteria. a, The *in vitro* binding assay was performed with *E. coli* and recombinant GP2-Fc and control hIgG-Fc proteins. Error bars indicate s.e.m. ($n = 3$). **b**, The GP2-binding capacity of *E. coli* was further examined using the parental K12 strain and *FimH*, *CsgA* or *FliC* knockout strains (ΔFimH, ΔCsgA or ΔFliC, respectively). Error bars indicate s.e.m. ($n = 3$). **c**, Interaction of recombinant GP2-Fc proteins with various commensal and pathogenic enterobacteria was examined by the *in vitro* binding assay. The binding index represents the fold change in the number of bacteria in hGP2-Fc or mGP2-Fc relative to that in control Fc. Error bars indicate s.e.m. (one-way analysis of variance followed by Tukey's test; $n = 3$ for all tested groups). **d**, After the ligated intestinal loop assay with GFP-*E. coli* (green), the whole-mount specimen of Peyer's patch was stained for GP2 (red), and analysed by deconvolution microscopy. Serial *X*–*Y* sections of whole-mount staining of an M cell from apical (image 1) to basal (image 9) domains are shown. Arrowheads indicate GFP-*E. coli* just being internalized into the M cell. The M-cell pocket is indicated by a dotted circular line (images 7–9). **e**, The *X*–*Z* image of an M cell at the position indicated by a dotted line in image 3 is shown. Arrows indicate GP2 densely clustered around GFP-*E. coli*. For three-dimensional imaging, see Supplementary Movie 2. **f**, After the ligated intestinal loop assay, the Peyer's patch was stained for GP2 (red) and a DC marker CD11c (blue). In this image, the GFP-*E. coli* was transcytosed by an M cell from the apical surface to the M-cell pocket, into which a DC has migrated to capture the bacterium. Left, top view. Right, side view. For three-dimensional imaging, see Supplementary Movie 4.

Y. enterocolitica, which gains entry into M cells through binding to β_1-integrin[22], between $Gp2^{+/+}$ and $Gp2^{-/-}$ mice (Fig. 3a, right). Taken together, these data underscore the importance of the binding of GP2 and FimH in the transcytosis of type-I-piliated bacteria by M cells.

It has been thought that the antigens transcytosed by M cells are transferred to immature DCs accumulating in the subepithelial dome (SED) region beneath the FAE[6]. The antigen-primed DCs would then undergo maturation and migrate to the T-cell-rich region in Peyer's patches for antigen presentation and subsequent initiation of antigen-specific mucosal immunity including IgA^+ B-cell formation[23]. We explored whether bacterial antigens transcytosed by means of the GP2-dependent pathway are captured by DCs. After the intestinal loop assay, we observed DCs capturing GFP-*E. coli* in the M-cell pocket, the microdomain formed by invagination of the basolateral plasma membrane (Fig. 2f and Supplementary Movie 4). Quantitative analysis showed that more than 90% of the translocated bacteria were captured by DCs (Supplementary Fig. 10).

We also examined whether GP2-dependent bacterial transcytosis contributes to the initiation of the antigen-specific immune response in Peyer's patches. We employed an established oral immunization model using recombinant *S.* Typhimurium expressing fragment C of tetanus toxoid (r*Salmonella*-ToxC) as an antigen[24]. We here developed the *FimH*-deletion mutant strain of r*Salmonella*-ToxC. These bacteria grew normally but lost the ability to bind GP2 recombinant protein (Fig. 4a), consistent with FimH-deficient *E. coli* (Fig. 2b). Correspondingly, a deficiency of FimH greatly lowered bacterial entry into Peyer's patches and the mesenteric lymph node (MLN) (Fig. 4b). As a consequence, the FimH-deficient strain induced a weak antigen-specific helper-T-cell (T_H) response in Peyer's patches (Fig. 4c) in comparison with its parental strain, resulting in attenuated antigen-specific faecal IgA and serum IgG production (Fig. 4d, e). Similarly, $Gp2^{-/-}$ mice failed to induce antigen-specific T_H-cell and antibody immune responses after oral immunization with $FimH^+$ r*Salmonella*-ToxC (Fig. 3b–d and Supplementary Fig. 11). This was not due to a defect in the immunological function of $Gp2^{-/-}$ mice, because splenic tetanus toxoid (TT)-specific T_H response was normally induced in these mice after systemic immunization (Supplementary Fig. 12). These observations demonstrate that GP2-dependent bacterial transcytosis is involved in immunosurveillance for $FimH^+$ bacteria in the intestinal lumen.

The identification of GP2 expression by M cells from Peyer's patches and its functional characterization support the hypothesis that M cells express bacterial pattern-recognition molecules on their

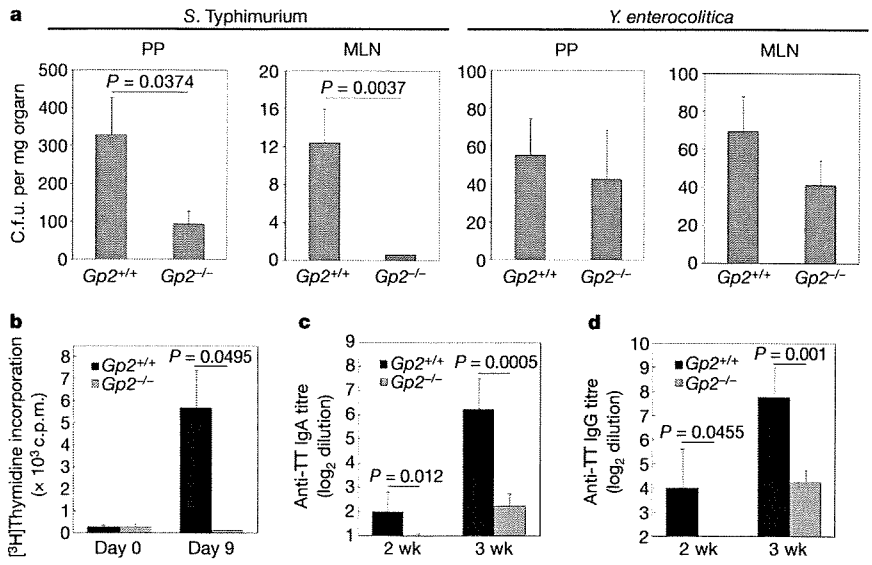

Figure 3 | GP2 is important for the induction of an antigen-specific mucosal immune response. **a**, $Gp2^{+/+}$ or $Gp2^{-/-}$ C57BL/6 mice were orally infected with 5×10^7 c.f.u. of *S.* Typhimurium or 10^9 c.f.u. of *Y. enterocolitica*. Peyer's patches and MLN were collected 24 h after the infection to prepare tissue homogenates. The colonies of culturable bacteria in the tissue homogenates were counted and normalized to the weight of tissue samples, and are shown as colony-forming units. Data from two independent experiments were pooled and are shown as means and s.e.m. (Mann–Whitney *U*-test, $n = 6$). **b–d**, $Gp2^{+/+}$ or $Gp2^{-/-}$ C57BL/6 mice were orally immunized with 5×10^7 c.f.u. of r*Salmonella*-ToxC ($FimH^+$ strain). **b**, CD4 T cells were prepared from Peyer's patches 9 days after oral immunization, and were co-cultured for 4 days with irradiated splenic antigen-presenting cells obtained from C57BL/6 mice in the presence of TT to examine the proliferative response. Data are shown as means and s.d. ($n = 3$, Mann–Whitney *U*-test) and are representative of three independent experiments. **c, d**, The presence of TT-specific IgA in faeces (**c**) and IgG in serum (**d**) at 2 and 3 weeks after oral immunization was evaluated by ELISA ($n = 4$; Student's *t*-test). Data are shown as means and s.d. and are representative of four independent experiments.

apical surface that efficiently bind luminal microorganisms. Moreover, GP2-mediated transcytosis is necessary for the initiation of antigen-specific mucosal immune responses against type-I-piliated bacteria (Supplementary Fig. 1). Recent studies demonstrate that the translocation of *Salmonella* into Peyer's patches is required for the initiation of antigen-specific IgA responses[25,26], whereas DC-mediated delivery of the bacteria from intestinal lamina propria to the MLN and the spleen is responsible for inducing an antigen-specific IgG response. Our data showed that GP2 or FimH deficiency moderately, but significantly, decreased the antigen-specific IgG response after oral immunization with r*Salmonella*-ToxC (Figs 3d and 4e), most probably as a result of attenuated bacterial translocation to the MLN (Figs 3a and 4b). These observations raise the possibility that the entry of type-I-piliated bacteria into M cells by means of the GP2–FimH system could also contribute to bacterial delivery to the MLN. An alternative, but not mutually exclusive, interpretation is that GP2 might also have a function in bacterial translocation to intestinal lamina propria. Given that the soluble form of GP2 is abundantly released from the exocrine pancreas into the gastrointestinal tract[13,27], the soluble GP2 might 'opsonize' luminal type-1-piliated bacteria and mediate efficient bacterial translocation at the lamina propria. Further study will be necessary to verify this speculation.

Our data therefore support the biological significance of antigen transcytosis by M cells in the front-line defence against enteric microbes by inducing mucosal immune responses. Future clarification of the GP2-mediated transcytotic mechanisms will define the

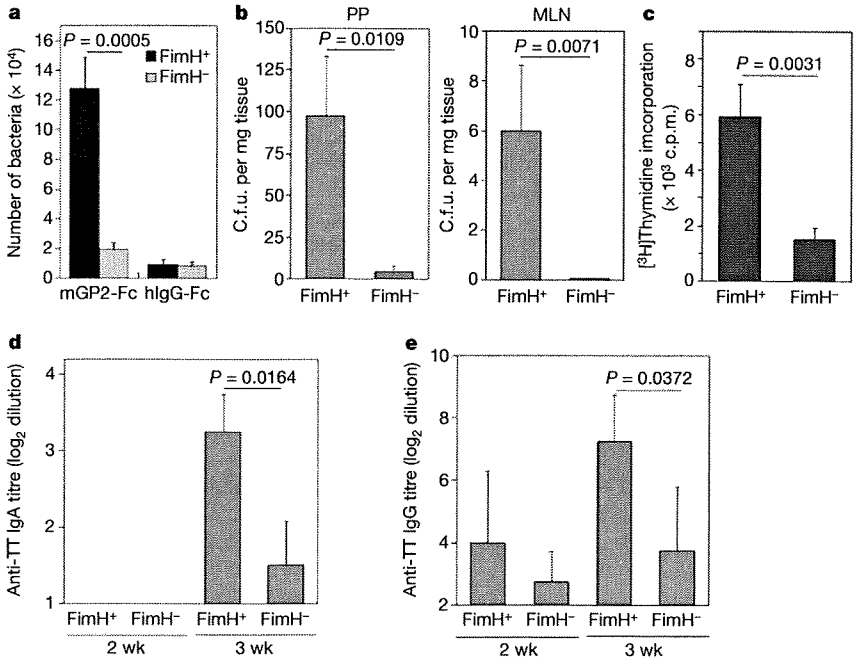

Figure 4 | Bacterial translocation into Peyer's patches and subsequent antigen-specific mucosal immune response markedly decreased in FimH-deficinet *Salmonella*. **a**, The *FimH* gene knockout ($FimH^-$) strain of r*Salmonella*-ToxC was developed as described in Methods. The *in vitro* binding assay was performed with parental ($FimH^+$) or $FimH^-$ r*Salmonella*-ToxC in microtitre plate immobilized with 5 μg ml^{-1} mGP2-Fc or control hIgG-Fc protein. Data are shown as means and s.d. ($n = 3$; Student's *t*-test). **b–e**, C57BL/6 mice were fed with 5×10^7 c.f.u. of $FimH^+$ or $FimH^-$ r*Salmonella*-ToxC. After 24 h, bacterial translocation to Peyer's patches and MLN was examined (**b**, $n = 5$; Mann–Whitney *U*-test). CD4 T cells were prepared from Peyer's patches 9 days after oral immunization, and were co-cultured for 4 days with irradiated splenic antigen-presenting cells obtained from the mice in the presence of TT to examine the proliferative response (**c**, $n = 3$; Student's *t*-test). The presence of TT-specific IgA in faeces (**d**) and IgG in serum (**e**) at 2 and 3 weeks after oral immunization were evaluated by ELISA ($n = 4$; Mann–Whitney *U*-test). Data are shown as means and s.d. and are representative of three independent experiments.

molecular basis of antigen transport by M cells and provide a new approach for 'M-cell-targeted' vaccination protocols.

METHODS SUMMARY

Animals. BALB/c and C57BL/6 mice were purchased from CLEA Japan. GP2-deficient mice were generated as described previously[28,29], and were backcrossed onto a C57BL/6 genetic background. Mice were maintained under specific pathogen-free conditions in the animal facilities of RIKEN and the University of Tokyo until use in experiments. All animal experiments were approved by the Animal Research Committees of RIKEN Yokohama Research Institute and the Institute of Medical Science, the University of Tokyo.

***In vitro* bacterial binding assay.** Recombinant mGP2-Fc, hGP2-Fc or control Fc proteins were immobilized in 96-well polystyrene microtitre plates by incubation overnight at 4 °C. After washing, the microtitre wells were incubated with 1% BSA in PBS for 2 h for blocking, and then incubated for 2 h with 10^6 colony-forming units (c.f.u.) of various bacteria in 1% BSA in PBS at 20–25 °C. After washing five times with sterile PBS, genomic DNA was extracted from bound bacteria with a QIAamp DNA kit (Qiagen). The copy number of 16S ribosomal RNA (rRNA) genes was determined by real-time qPCR with SYBR Premix Ex Taq (TaKaRa) and specific primers for universal 16S rRNA gene[30].

Ligated intestinal loop assay. Mice were anaesthetized with avertin and kept warm on a 37 °C warming pad during the assay. GFP-*E. coli* or GFP-*E. coli* (*FimH*$^-$) (10^8 c.f.u.) or 50 μg ml^{-1} anti-mouse GP2 mAb (clone 2F11-C3) were injected into the ligated intestinal loop. After incubation for 30–60 min, the mice were killed and Peyer's patches were excised from the intestine. Specimens were observed with a DM-IRE2 confocal laser scanning microscope (Leica Microsystems) or a DeltaVision Restoration deconvolution microscope (Applied Precision).

Full Methods and any associated references are available in the online version of the paper at www.nature.com/nature.

Received 16 August; accepted 23 September 2009.

1. Cerutti, A. & Rescigno, M. The biology of intestinal immunoglobulin A responses. *Immunity* **28**, 740–750 (2008).
2. Fagarasan, S. *et al.* Critical roles of activation-induced cytidine deaminase in the homeostasis of gut flora. *Science* **298**, 1424–1427 (2002).
3. Peterson, D. A., McNulty, N. P., Guruge, J. L. & Gordon, J. I. IgA response to symbiotic bacteria as a mediator of gut homeostasis. *Cell Host Microbe* **2**, 328–339 (2007).
4. Craig, S. W. & Cebra, J. J. Peyer's patches: an enriched source of precursors for IgA-producing immunocytes in the rabbit. *J. Exp. Med.* **134**, 188–200 (1971).
5. Owen, R. L. & Jones, A. L. Epithelial cell specialization within human Peyer's patches: an ultrastructural study of intestinal lymphoid follicles. *Gastroenterology* **66**, 189–203 (1974).
6. Neutra, M. R., Mantis, N. J. & Kraehenbuhl, J. P. Collaboration of epithelial cells with organized mucosal lymphoid tissues. *Nature Immunol.* **2**, 1004–1009 (2001).
7. Nochi, T. *et al.* A novel M cell-specific carbohydrate-targeted mucosal vaccine effectively induces antigen-specific immune responses. *J. Exp. Med.* **204**, 2789–2796 (2007).
8. Sirard, J. C., Niedergang, F. & Kraehenbuhl, J. P. Live attenuated *Salmonella*: a paradigm of mucosal vaccines. *Immunol. Rev.* **171**, 5–26 (1999).
9. Sansonetti, P. J. & Phalipon, A. M cells as ports of entry for enteroinvasive pathogens: mechanisms of interaction, consequences for the disease process. *Semin. Immunol.* **11**, 193–203 (1999).
10. Kraehenbuhl, J. P. & Neutra, M. R. Epithelial M cells: differentiation and function. *Annu. Rev. Cell Dev. Biol.* **16**, 301–332 (2000).
11. Hase, K. *et al.* Distinct gene expression profiles characterize cellular phenotypes of follicle-associated epithelium and M cells. *DNA Res.* **12**, 127–137 (2005).
12. Terahara, K. *et al.* Comprehensive gene expression profiling of Peyer's patch M cells, villous M-like cells, and intestinal epithelial cells. *J. Immunol.* **180**, 7840–7846 (2008).
13. Hoops, T. C. & Rindler, M. J. Isolation of the cDNA encoding glycoprotein-2 (GP-2), the major zymogen granule membrane protein. Homology to uromodulin/Tamm–Horsfall protein. *J. Biol. Chem.* **266**, 4257–4263 (1991).
14. Verbrugghe, P., Kujala, P., Waelput, W., Peters, P. J. & Cuvelier, C. A. Clusterin in human gut-associated lymphoid tissue, tonsils, and adenoids: localization to M cells and follicular dendritic cells. *Histochem. Cell Biol.* **129**, 311–320 (2008).
15. Fukuoka, S., Freedman, S. D., Yu, H., Sukhatme, V. P. & Scheele, G. A. GP-2/THP gene family encodes self-binding glycosylphosphatidylinositol-anchored proteins in apical secretory compartments of pancreas and kidney. *Proc. Natl Acad. Sci. USA* **89**, 1189–1193 (1992).
16. Mo, L. *et al.* Ablation of the Tamm–Horsfall protein gene increases susceptibility of mice to bladder colonization by type 1-fimbriated *Escherichia coli*. *Am. J. Physiol. Renal Physiol.* **286**, F795–F802 (2004).
17. Pizarro-Cerda, J. & Cossart, P. Bacterial adhesion and entry into host cells. *Cell* **124**, 715–727 (2006).
18. Yu, S. & Lowe, A. W. The pancreatic zymogen granule membrane protein, GP2, binds *Escherichia coli* type 1 fimbriae. *BMC Gastroenterol.* **9**, 58 (2009).
19. Ewen, S. W. *et al.* *Salmonella enterica* var Typhimurium and *Salmonella enterica* var Enteritidis express type 1 fimbriae in the rat *in vivo*. *FEMS Immunol. Med. Microbiol.* **18**, 185–192 (1997).
20. McDonald, D. *et al.* Recruitment of HIV and its receptors to dendritic cell–T cell junctions. *Science* **300**, 1295–1297 (2003).
21. Tanaka, Y. *et al.* T helper type 2 differentiation and intracellular trafficking of the interleukin 4 receptor-α subunit controlled by the Rac activator Dock2. *Nature Immunol.* **8**, 1067–1075 (2007).
22. Clark, M. A., Hirst, B. H. & Jepson, M. A. M-cell surface β1 integrin expression and invasin-mediated targeting of *Yersinia pseudotuberculosis* to mouse Peyer's patch M cells. *Infect. Immun.* **66**, 1237–1243 (1998).
23. Iwasaki, A. & Kelsall, B. L. Localization of distinct Peyer's patch dendritic cell subsets and their recruitment by chemokines macrophage inflammatory protein (MIP)-3α, MIP-3β, and secondary lymphoid organ chemokine. *J. Exp. Med.* **191**, 1381–1394 (2000).
24. VanCott, J. L. *et al.* Regulation of mucosal and systemic antibody responses by T helper cell subsets, macrophages, and derived cytokines following oral immunization with live recombinant *Salmonella*. *J. Immunol.* **156**, 1504–1514 (1996).
25. Martinoli, C., Chiavelli, A. & Rescigno, M. Entry route of *Salmonella typhimurium* directs the type of induced immune response. *Immunity* **27**, 975–984 (2007).
26. Hashizume, T. *et al.* Peyer's patches are required for intestinal immunoglobulin A responses to *Salmonella* spp. *Infect. Immun.* **76**, 927–934 (2008).
27. Rindler, M. J. & Hoops, T. C. The pancreatic membrane protein GP-2 localizes specifically to secretory granules and is shed into the pancreatic juice as a protein aggregate. *Eur. J. Cell Biol.* **53**, 154–163 (1990).
28. Kobayashi, K., Yanagihara, K., Ishiguro, K. & Fukuoka, S. GP2/THP gene family of self-binding, GPI-anchored proteins forms a cluster at chromosome 7F1 region in mouse genome. *Biochem. Biophys. Res. Commun.* **322**, 659–664 (2004).
29. Yu, S., Michie, S. A. & Lowe, A. W. Absence of the major zymogen granule membrane protein, GP2, does not affect pancreatic morphology or secretion. *J. Biol. Chem.* **279**, 50274–50279 (2004).
30. Greisen, K., Loeffelholz, M., Purohit, A. & Leong, D. PCR primers and probes for the 16S rRNA gene of most species of pathogenic bacteria, including bacteria found in cerebrospinal fluid. *J. Clin. Microbiol.* **32**, 335–351 (1994).

Supplementary Information is linked to the online version of the paper at www.nature.com/nature.

Acknowledgements We thank K. Kanno and A. Yamada for help in immunoelectron microscopy; Y. Yamada for secretarial assistance; M. Ohmae for technical assistance; H. Watarai for pertinent advice and discussion; P. D. Burrows, T. Takemori, S. Yamasaki and H. Kitamura for critical review of the manuscript; and the National BioResource Project (NIG, Japan) for *E. coli* (the Keio collection). This study was supported in part by Grants-in-Aid for Young Scientists (B) (K.H.), Scientific research (B) (H.O.), Scientific Research in Priority Areas (H.O. and K.H.), and Scientific Research on Innovative Areas (H.O.) from the Ministry of Education, Culture, Sports, Science and Technology of Japan, the Takeda Science Foundation (K.H.), and NIH awards DK56339 and DK43294 (A.W.L.).

Author Contributions K. Hase and K. Kawano designed and performed the experiments, analysed the data and wrote the manuscript. T.N., G.S.P., S.F., M.E., K. Kadokura, Y.F., S. Kawano, A.Y., G.N., S. Kimura, M.I., K. Hamura, S.W. and H.K. contributed to the experimental work, and T.M. helped in data analysis. T.T. developed the FimH-deficient strain of r*Salmonella*-ToxC. K.I. prepared bacteria. S-I.F. and A.W.L. provided GP2-deficient mice. H.O. supervised the project and made significant contributions to the manuscript.

Author Information Reprints and permissions information is available at www.nature.com/reprints. Correspondence and requests for materials should be addressed to H.O. (ohno@rcai.riken.jp).

METHODS

Quantitative PCR. Total RNA was prepared from FAE and villus epithelium as described previously[11]. Mouse *Gp2* gene expression was examined by real-time qPCR with SYBR Premix Ex Taq (TaKaRa) and specific primers, mGP2 5′-GATA CTGCACAGACCCCTCCA-3′ (forward) and 5′-GCAGTTCCGGTCATTGAGGT A-3′ (reverse), as described previously[31]. The mouse *Gp2* expression level was normalized to that of the glyceraldehyde-3-phosphate dehydrogenase gene in each tissue, and data are expressed as fold change in FAE compared with that in villus epithelium.

cDNA clones and plasmid construction. To obtain constructs for fusion proteins of mouse (m) or human (h) GP2 with the Fc segment of human IgG1, cDNAs corresponding to the amino-terminal region of GP2 lacking the transmembrane domain were amplified by PCR with a RIKEN FANTOM clone 2310037I18 or human FAE, respectively, as template. Primers used were as follows: mGP2, 5′-GAAGATCTACCATGAAAAGGATGGTGGGTT-3′ (forward) and 5′-CCGCT CGAGTGTAGTGTGGGGAGTCCCC-3′ (reverse); hGP2, 5′-CGCGGATCCACC ATGGAAAGGATGGTGGGC-3′ (forward) and 5′-CCGCTCGAGTCCATTCAT GACACCGGGAGA-3′ (reverse). cDNA fragments were inserted into the *Bam*HI/*Xho*I cloning sites of a pcDNA3 expression vector (Invitrogen) containing a fragment encoding the Fc segment of human IgG1 to obtain mGP2-Fc and hGP2-Fc. For *in situ* hybridization, an N-terminal fragment of mouse and human GP2 (GP2-N) was prepared by using mouse or human GP2-Fc/pcDNA3 vectors and the following primers: mGP2-N, 5′-GAAGATCTCGATTCATCAGTTGCATGGTG-3′ (forward) and 5′-CCGCTCGAGGAAACCCATACCTCCCAGCA-3′ (reverse); hGP2-N, 5′-CGCGGATCCGCGATAAAAACATGAGCGGC-3′ (forward) and 5′-CCGCTCGAGCTCTCCAGAATGTTCCTGCAG-3′ (reverse). The cDNA fragments obtained were inserted into the *Bam*HI/*Xho*I cloning sites of the pcDNA3 expression vector.

***In situ* hybridization.** Digoxigenin-labelled RNA probes were prepared by *in vitro* transcription with SP6 RNA polymerase (Roche), using mouse and human GP2-N/pcDNA3 plasmid vectors digested with *Bam*HI as templates. Paraffin-embedded tissue sections prepared from murine Peyer's patches were deparaffinized, treated with proteinase K and hybridized for 16 h with 100 ng ml^{-1} digoxigenin-labelled RNA probes at 60 °C. Specific binding was detected by incubation with alkaline phosphatase-conjugated anti-digoxigenin antibody (Roche Diagnostics) for 2 h at room temperature, and revealed with purple alkaline phosphatase substrate overnight (Genostaff). The sections were counterstained with UEA-1 or nuclear fast red. For *in situ* hybridization of hGP2, endoscopic biopsies or surgical sections were obtained from non-inflamed terminal ileum containing lymphoid follicles from patients who had previously given informed consent. Biopsy samples were fixed with 4% buffered formalin and hybridized with the hGP2-specific antisense probe or control sense probe as described above for mouse samples. These studies were approved by the Committee on Human Subjects in RIKEN and Tokyo Women's Medical University.

Recombinant protein preparation. Human embryonic kidney (HEK293T) cells were transiently transfected with the Fc-fusion expression vectors prepared as above and cultured for 7–10 days. Recombinant proteins secreted into the culture supernatant were purified with a HiTrap protein A HP affinity column (GE Healthcare). The recombinant fusion proteins mGP2(ΔTM)-Fc and hGP2(ΔTM)-Fc were used in the assay for bacterial binding and for mAb preparation.

Development of GP2-specific antibodies. Rabbit polyclonal antibodies specific for mGP2 were generated in response to a keyhole-limpet haemocyanin-conjugated 16-amino-acid peptide (CSEELGEYHVYKLQGT) corresponding to residues 154–169 of mouse GP2. Rat anti-mouse GP2 IgG2a (clones 2F11-C3 and 1F5-H9) and mouse anti-human GP2 IgG1 (clone 3G7-H9) mAbs were raised by immunization with recombinant mouse or human GP2-Fc fusion proteins, respectively.

Immunoblotting. HeLa cells transfected with full-length mGP2/pcDNA3 plasmid or tissues from 12-week-old BALB/c mice were homogenized in ice-cold lysis buffer containing 20 mM Tris-HCl pH 7.5, 150 mM NaCl, 1 mM EDTA, 0.1% Triton X-100 and a protease inhibitor cocktail (Roche). Each homogenate was centrifuged at 10,000*g* for 10 min at 4 °C. The supernatants were separated by SDS–PAGE and then transferred to an Immobilon-P membrane (Millipore). GP2 protein was probed with anti-mGP2 polyclonal antiserum or pre-immune serum. Specific binding of the primary antibody was detected with horseradish-peroxidase-conjugated secondary antibody followed by Immobilon Western HRP Substrate (Millipore).

Immunofluorescent staining. To detect mouse GP2, paraffin sections of Peyer's patches, isolated lymphoid follicles or caecal or colonic patches were dehydrated and treated with anti-mouse GP2 mAbs described above. The binding of primary Abs was revealed with the TSA fluorescence system (PerkinElmer) in accordance with the manufacturer's instructions. The sections were further stained with rhodamine-labelled UEA-1 (Vector Laboratories) and counterstained with 4,6-diamidino-2-phenylindole. Because specimens of human Peyer's patches showed autofluorescence, specific binding of the primary antibody was revealed with the DAB substrate chromogen system (Dako).

For whole-mount staining, mouse Peyer's patches were excised from the small intestine and washed vigorously in ice-cold PBS, then fixed and permeabilized with a Cytofix/Cytoperm kit (BD Bioscience). The whole-mount specimens of Peyer's patches were then stained with anti-GP2 mAb (2F11-C3) followed by secondary antibodies conjugated with Alexa488 or Alexa594. In some experiments the specimens were further stained with rhodamine-labelled UEA-1 and Alexa633-labelled phalloidin. The specimens were embedded in a 30% solution of glycerol in PBS, and analysed with a DM-IRE2 confocal laser scanning microscope (Leica Microsystems) and a DeltaVision Restoration deconvolution microscope (Applied Precision).

Immunoelectron microscopy. Excised tissues were fixed by immersion in 4% paraformaldehyde/0.1% glutaraldehyde. Immunoelectron microscopy was performed on cryo-ultrathin sections as described previously[32].

Preparation of GFP-expressing *E. coli* and *S.* Typhimurium. *E. coli* K-12, its *FimH*-deficient mutant, and *S.* Typhimurium were transformed with the bacterial GFP expression vector pKKGFP[33] to generate GFP-*E. coli* and GFP-*E. coli* ΔFimH, respectively. The GFP–*S.* Typhimurium[33] was provided by J. P. Kraehenbuhl.

Preparation of FimH-deletion mutant of r*Salmonella*-ToxC. The *fimH* deletion mutants of *Salmonella* Typhimurium harbouring toxC were constructed by using the method and plasmids of refs 34, 35 with slight modification. In brief, *S.* Typhimurium harbouring pACBSR was transformed with PCR product, which was created on pKD4 with primers S-fimH-H1 (5′-CCTGTATCCGTCCGGCG TCATAAAAGGAAAAATAGAGATGGTGTAGGCTGGAGCTGCTTC-3′) and S-fimH-H2 (5′-TAGCGATGAAAACGCGCCGAAGGATCATTATGCCTCCTT ACCATATGAATATCCTCCTTA-3′). After growth in Luria–Bertani medium containing arabinose, kanamycin-resistant transformants were selected.

Immunization. The procedure of oral immunization with r*Salmonella*-ToxC is described elsewhere[24]. In brief, $Gp2^{+/+}$ or $Gp2^{-/-}$ mice were fed with 5×10^7 c.f.u. of the parental or FimH-deletion mutant strain of r*Salmonella*-ToxC (*aroA*$^-$, *aroD*$^-$) in 200 μl of PBS. Alternatively, mice received an intraperitoneal injection with 5×10^5 c.f.u. of r*Salmonella*-ToxC for systemic immunization. To evaluate antigen-specific T-cell response, CD4 T cells purified from Peyer's patches and splenic cell suspension by magnetic cell separation (MACS; Miltenyi Biotec) with microbead-conjugated anti-CD4 were co-cultured with irradiated splenocytes from C57BL/6 mice in the presence of 100 μg ml^{-1} TT (Biken Foundation) for 3 days. [^{3}H]Thymidine (Amersham) were added to culture media 16 h before harvest to measure T-cell proliferation. The antibody titre specific for TT or *Salmonella* membrane fraction in serum and faecal extracts was measured by ELISA as described previously[36,37].

CFU assay after oral infection. *S.* Typhimurium carrying a nalidixic acid resistance gene (χ3306)[38] was a gift from H. Matsui. $Gp2^{+/+}$ or $Gp2^{-/-}$ mice were fed with 5×10^7 c.f.u. of *S.* Typhimurium χ3306 or 10^9 c.f.u. of *Y. enterocolitica* WA (ATCC 27729)[39]. After 24 h, Peyer's patches and ileal tissue were dissected and incubated at room temperature in sterile PBS containing 100 μg ml^{-1} gentamicin for 30 min with gentle shaking. The tissues were weighed and homogenized in sterile PBS. The MLN was also removed and homogenized. The homogenates were serially diluted in sterile PBS and plated on a Luria–Bertani agar plate containing 25 μg ml^{-1} nalidixic acid or a *Yersinia*-selective agar plate (Oxoid) to determine colony-forming units.

Statistical analyses. Differences between two or more groups were analysed by Student's *t*-test or a one-way analysis of variance followed by Tukey's test, respectively. When variances were not homogeneous, the data were analysed by Mann–Whitney *U*-test or Kruskal–Wallis ANOVA followed by a Scheffé test. All statements of significant differences show a 5% level of probability.

31. Hase, K. *et al.* The membrane-bound chemokine CXCL16 expressed on follicle-associated epithelium and M cells mediates lympho-epithelial interaction in GALT. *J. Immunol.* **176**, 43–51 (2006).
32. Waguri, S. & Komatsu, M. Biochemical and morphological detection of inclusion bodies in autophagy-deficient mice. *Methods Enzymol.* **453**, 181–196 (2009).
33. Hopkins, S. A., Niedergang, F., Corthesy-Theulaz, I. E. & Kraehenbuhl, J. P. A recombinant *Salmonella typhimurium* vaccine strain is taken up and survives within murine Peyer's patch dendritic cells. *Cell. Microbiol.* **2**, 59–68 (2000).
34. Herring, C. D., Glasner, J. D. & Blattner, F. R. Gene replacement without selection: regulated suppression of amber mutations in *Escherichia coli*. *Gene* **311**, 153–163 (2003).
35. Datsenko, K. A. & Wanner, B. L. One-step inactivation of chromosomal genes in *Escherichia coli* K-12 using PCR products. *Proc. Natl Acad. Sci. USA* **97**, 6640–6645 (2000).
36. Jackson, R. J. *et al.* Optimizing oral vaccines: induction of systemic and mucosal B-cell and antibody responses to tetanus toxoid by use of cholera toxin as an adjuvant. *Infect. Immun.* **61**, 4272–4279 (1993).
37. Yamamoto, M. *et al.* Alternate mucosal immune system: organized Peyer's patches are not required for IgA responses in the gastrointestinal tract. *J. Immunol.* **164**, 5184–5191 (2000).
38. Gulig, P. A., Doyle, T. J., Hughes, J. A. & Matsui, H. Analysis of host cells associated with the Spv-mediated increased intracellular growth rate of *Salmonella typhimurium* in mice. *Infect. Immun.* **66**, 2471–2485 (1998).
39. Carter, P. B. & Collins, F. M. Experimental *Yersinia enterocolitica* infection in mice: kinetics of growth. *Infect. Immun.* **9**, 851–857 (1974).

The Journal of Immunology

RANKL Is Necessary and Sufficient to Initiate Development of Antigen-Sampling M Cells in the Intestinal Epithelium

Kathryn A. Knoop, Nachiket Kumar, Betsy R. Butler, Senthilkumar K. Sakthivel, Rebekah T. Taylor, Tomonori Nochi, Hisaya Akiba, Hideo Yagita, Hiroshi Kiyono and Ifor R. Williams

J. Immunol. 2009;183;5738-5747; originally published online Oct 14, 2009;
doi:10.4049/jimmunol.0901563
http://www.jimmunol.org/cgi/content/full/183/9/5738

The Journal of Immunology is published twice each month by The American Association of Immunologists, Inc., 9650 Rockville Pike, Bethesda, MD 20814-3994.

Print ISSN: 0022-1767 Online ISSN: 1550-6606.

RANKL Is Necessary and Sufficient to Initiate Development of Antigen-Sampling M Cells in the Intestinal Epithelium[1]

Kathryn A. Knoop,* Nachiket Kumar,* Betsy R. Butler,* Senthilkumar K. Sakthivel,* Rebekah T. Taylor,* Tomonori Nochi,† Hisaya Akiba,‡ Hideo Yagita,‡ Hiroshi Kiyono,† and Ifor R. Williams[2]*

Microfold cells (M cells) are specialized epithelial cells situated over Peyer's patches (PP) and other organized mucosal lymphoid tissues that transport commensal bacteria and other particulate Ags into intraepithelial pockets accessed by APCs. The TNF superfamily member receptor activator of NF-κB ligand (RANKL) is selectively expressed by subepithelial stromal cells in PP domes. We found that RANKL null mice have <2% of wild-type levels of PP M cells and markedly diminished uptake of 200 nm diameter fluorescent beads. Ab-mediated neutralization of RANKL in adult wild-type mice also eliminated most PP M cells. The M cell deficit in RANKL null mice was corrected by systemic administration of exogenous RANKL. Treatment with RANKL also induced the differentiation of villous M cells on all small intestinal villi with the capacity for avid uptake of *Salmonella* and *Yersinia* organisms and fluorescent beads. The RANK receptor for RANKL is expressed by epithelial cells throughout the small intestine. We conclude that availability of RANKL is the critical factor controlling the differentiation of M cells from RANK-expressing intestinal epithelial precursor cells. *The Journal of Immunology,* 2009, 183: 5738–5747.

The organized lymphoid tissues of the intestine are inductive sites for both the generation of secretory IgA and the generation of T cell tolerance to Ags present in the intestinal lumen, including those derived from food and the commensal flora (1, 2). The follicle-associated epithelium (FAE)[3] that covers the lymphoid follicles of both Peyer's patches (PP) and isolated lymphoid follicles (ILF) contains specialized epithelial cells known as microfold cells (M cells) that provide a portal for efficient sampling of particulate Ags from the lumen (3, 4). Ags acquired through this major pathway for Ag sampling in the intestine are delivered into intraepithelial pockets within the M cells that lymphocytes and APC access from the subepithelial dome region. The M cell-mediated Ag-sampling pathway has a central role in the development of immune responses to both pathogenic bacteria and commensal bacteria. Production of protective fecal IgA in mice after oral infection with invasive *Salmonella* species requires the presence of PP with M cells (5, 6). In addition, some commensal bacteria internalized through M cells are passed into dendritic cells (DC) that travel with their cargo to the draining mesenteric lymph node, leading to both IgA Ab production and establishment of T cell tolerance (7). M cells also promote the development of T cell tolerance to Ags acquired through the gastrointestinal tract. Targeting OVA to mouse M cells via the reovirus sigma 1 protein resulted in enhanced development of oral tolerance in $CD4^+$ T cells (8). Although most M cells in the small intestine of wild-type mice are localized to the FAE of PP and ILF, occasional villi contain clusters of cells known as villous M cells that exhibit all the major defining characteristics of PP M cells including reactivity with the *Ulex europaeus* agglutinin-I (UEA-I) lectin recognizing α(1,2)-fucose, stubby microvilli, and the capacity to ingest and transcytose particles the size of bacteria (9).

Although the basic functional and ultrastructural features of M cells were initially described over 30 years ago (10), many basic questions about M cell differentiation and function remain unsolved. It has been proposed that specific factors released from the lymphoid microenvironment immediately beneath the FAE have the potential to elicit M cell differentiation in the FAE and promote the function of M cells, but specific signaling mediators with such activity have not been identified to date (11, 12). Debate continues on whether M cells are a distinct lineage arising from crypt stem cells like other differentiated intestinal epithelial cells or whether M cells can instead arise from normal FAE enterocytes with the plasticity to transition into M cells upon encountering the right set of stimuli (13–15).

RANKL (receptor activator of NF-κB ligand) is a member of the TNF superfamily (16) that is also referred to as TNF-related activation-induced cytokine and TNFSF11. Like TNF-α, RANKL is initially synthesized as a transmembrane protein that can be released from the cell surface following cleavage by one of several metalloproteases (17, 18). RANKL signals through its receptor RANK (receptor activator of NF-κB) and a downstream pathway that involves TRAF6 and the activation of NF-κB (19, 20). Osteoprotegerin is a soluble decoy receptor for RANKL that allows for tight regulation of the circulating levels of RANKL (21). A

*Department of Pathology and Laboratory Medicine, Emory University School of Medicine, Atlanta, GA 30322; †Division of Mucosal Immunology, Department of Microbiology and Immunology, University of Tokyo, Tokyo, Japan; and ‡Department of Immunology, Juntendo University School of Medicine, Tokyo, Japan

Received for publication May 21, 2009. Accepted for publication September 3, 2009.

The costs of publication of this article were defrayed in part by the payment of page charges. This article must therefore be hereby marked *advertisement* in accordance with 18 U.S.C. Section 1734 solely to indicate this fact.

[1] This work was supported by grants from the National Institutes of Health (DK64730 to I.R.W. and DK64399 supporting the Imaging Core Facility of the Emory Digestive Diseases Research Development Center) and the Crohn's & Colitis Foundation of America (Senior Research Award to I.R.W.).

[2] Address correspondence and reprint requests to Dr. Ifor R. Williams, Department of Pathology and Laboratory Medicine, Emory University School of Medicine, Whitehead Bldg. 105D, 615 Michael Street, Atlanta, GA 30322. E-mail address: irwilli@emory.edu

[3] Abbreviations used in this paper: FAE, follicle-associated epithelium; PP, Peyer's patch; ILF, isolated lymphoid follicle; M cell, microfold cell; DC, dendritic cell; RANK, receptor activator of NF-κB; RANKL, RANK ligand; mTEC, medullary thymic epithelial cell; GST, glutathione S-transferase; UEA-I, *Ulex europaeus* agglutinin-I; DAPI, 4′,6-diamidino-2-phenylindole.

www.jimmunol.org/cgi/doi/10.4049/jimmunol.0901563

major breakthrough in establishing a biological role for RANKL-RANK interactions was the discovery that RANKL signaling through RANK is required for normal osteoclast function (22, 23). Mice deficient in either RANKL or RANK have osteopetrosis and severe skeletal abnormalities because they lack the number of osteoclasts needed to remodel bone normally. RANKL-RANK signaling is also involved in several other critical biological processes including development of lymph nodes, development of medullary thymic epithelial cells (mTEC), mammary gland lactation, and provision of survival signals to DCs (22–27). The absence of all lymph nodes in RANKL-deficient mice demonstrates that RANKL is an essential mediator in lymphoid organogenesis (22, 23). RANKL induces lymphotoxin $\alpha_1\beta_2$ expression by lymphoid tissue inducer cells in the lymph node anlage (28). RANKL is not required for PP development, but the reduced size of PP reported in two independent lines of RANKL-deficient mice indicates that RANKL contributes to normal PP development (22, 23). Functional studies of PP were not done as part of the initial characterization of these mice.

We previously showed that RANKL is selectively expressed by stromal cells in the subepithelial dome region beneath the FAE of both PP and ILF (29). Stromal cells with phenotypic characteristics similar to neonatal lymph node organizer cells including RANKL expression were recently identified in multiple secondary lymphoid tissues including mucosal-associated lymphoid tissues and lymph nodes (30). The polarized pattern of RANKL expression by stromal cells beneath the FAE of PP and ILF suggested a possible function for RANKL in regulating the induction of mucosal immune responses to particulate luminal Ags taken up through the FAE. In this study, we evaluated the function of PP in RANKL null mice and found that absence of RANKL is associated with loss of the vast majority of UEA-I$^+$ M cells in the FAE. The depletion of M cells correlated with a profound functional defect in uptake from the intestinal lumen of fluorescent beads used as model particulate Ags. Systemic administration of exogenous-soluble RANKL restored functional UEA-I$^+$ M cells to the PP of RANKL null mice and simultaneously led to widespread induction of functional M cells on the epithelium covering small intestinal villi in both RANKL null mice and wild-type mice. These findings demonstrate that the RANKL-RANK pathway plays a pivotal nonredundant role in establishing the M cell-mediated pathway of Ag acquisition and handling.

Materials and Methods

Mice

Mice carrying a RANKL null mutation on a C57BL/6 background (31) obtained from Dr. Yongwon Choi at the University of Pennsylvania (Philadelphia, PA) were used to establish a breeding colony in a conventional specific pathogen free mouse facility at Emory University. Serological sentinel testing in this facility did not include routine testing for *Helicobacter* or *Pasteurella* species, but no infections attributed to these opportunistic pathogens were demonstrated in the colony of RANKL null mice or their controls. Because RANKL null mice lack teeth, weanling null mice born in this colony are routinely given powdered mouse chow. Mice heterozygous for the RANKL null mutation were also backcrossed to BALB/c mice (Taconic Farms) for a total of four generations. Male C57BL/6 RANKL$^{+/-}$ mice and female BALB/c RANKL$^{+/-}$ mice were intercrossed to produce RANKL null mice and littermate controls on a background roughly equivalent to (C57BL/6 × BALB/c)F_1 mice. RANKL null mice on this "F_1 equivalent" genetic background are closer in weight to their heterozygous and wild-type littermates and less likely to die prematurely compared with RANKL null mice on the two inbred backgrounds. Experiments using RANKL null mice were done with mice on a C57BL/6 background mice, a (C57BL/6 × BALB/c)F_1 background, or a mixed C57BL/6 and BALB/c background, as indicated in the figure legends. BALB/c mice (Taconic Farms) were used for experiments examining induction of villous M cells by RANKL in wild-type mice and the effects of anti-RANKL mAb on PP M cells. All animal studies were reviewed and approved by the Emory University Institutional Animal Care and Use Committee.

Recombinant mouse RANKL

A bacterial expression construct encoding a glutathione S-transferase (GST) fusion protein containing amino acids 137–316 of mouse RANKL was assembled in the pGEX-5X-1 vector (GE Healthcare) using a modification of a previously described method (32). The primers 5′-CAC CCCCGGGTCAGCGCTTCTCAGGAGCT-3′ and 5′-CTCGAGTCAG TCTATGTCCTGAAC-3′ were used to PCR amplify a cDNA clone for mouse RANKL (Open Biosystems). After the PCR product was cloned into the pENTR-D-TOPO cloning vector (Invitrogen) and sequenced, the *SmaI-XhoI* fragment was subcloned into pGEX-5X-1. The construct was transformed into the BL21 *Escherichia coli* strain (Stratagene) for fusion protein expression. The cultures were induced with 20 μM IPTG for 16 h at 20°C and the GST-RANKL purified from bacterial lysate by affinity chromatography on a GSTrap FF column (GE Healthcare) followed by dialysis against multiple changes of PBS. Recombinant GST used as a control was prepared by the same method using empty pGEX-5X-1. Biological activity of the GST-RANKL fusion protein was confirmed by its ability to induce differentiation of the RAW264.7 macrophage line (American Type Culture Collection) into multinucleate osteoclasts positive for tartrate resistant acid phosphatase. The GST-RANKL fusion protein was administered to RANKL null mice by daily i.p. or s.c. injections of 50 to 250 μg per day for up to 7 days. Recombinant GST prepared from empty pGEX-5X-1 vector was used as a control for GST-RANKL.

Bacterial strains

A wild-type strain of *Salmonella enterica* serovar Typhimurium (SL3201) transformed with the DsRed-Express plasmid (Clontech) encoding a cytoplasmic red fluorescent protein was provided by Dr. Andrew Neish at Emory University (Atlanta, GA). A *Yersinia enterocolitica* isolate (ATCC 29913) was purchased from the American Type Culture Collection. For experiments involving injection of bacteria into isolated intestinal loops, these bacteria were grown overnight in LB broth, washed in PBS, and fixed in 2% paraformaldehyde for 1 h. The fixed *Yersinia* were then labeled with Alexa 546-succidymyl ester (Molecular Probes) for 1 h at room temperature following the manufacturer's suggestions.

In vivo assessment of M cell uptake of fluorescent beads and bacteria

The uptake of 200-nm diameter fluorescent polystyrene latex nanoparticles (Fluoresbrite YG; Polysciences) and fluorescent bacteria by M cells in the FAE of individual PP or by villous M cells induced by exogenous RANKL treatment was assessed by either oral gavage or by using a modification of previously described isolated small intestinal loop models (33, 34). In oral gavage experiments examining uptake of the by RANKL-induced villous M cells, aliquots of 1×10^{11} 200 nm diameter nanoparticles in a volume of 200 μl were fed to the mice. To prepare isolated small intestinal loops, mice were anesthetized using an isoflurane vaporizer. After opening the peritoneum through a longitudinal midline incision, two or three segments of small intestine measuring 2–5 cm in length and containing either a single PP (to assess PP M cell uptake) or no PP (to assess villous M cell uptake) were tied off with nylon filament. For bead uptake studies, the loops were injected with 200–400 μl of a suspension of 200 nm nanoparticles diluted in PBS to a concentration of 1×10^{11} beads/ml and returned to the peritoneal cavity. The mice were euthanized 90 to 120 min after the loops were injected, and the injected intestinal segments were excised, washed in 0.5% Tween 20-PBS, fixed in 4% paraformaldehyde in PBS for 15 min, and embedded in OCT. Frozen sections cut from these intestinal segments were examined by microscopy after counterstaining with 4′,6-diamidino-2-phenylindole (DAPI), leaving out a cold acetone fixation step because acetone dissolved the polystyrene Fluoresbrite beads, preventing their visualization. For bacterial uptake studies, loops containing no PP were injected with 300 to 500 μl of bacterial suspension at a concentration of 5×10^9 organisms/ml. After 120 min, the mice were euthanized and the intestine tissue within the loop was embedded in OCT as a Swiss roll. Frozen sections from this tissue were fixed with −20°C acetone since this fixation did not interfere with detection of the fluorescent bacteria.

Abs and lectins

mAbs for staining were purchased from eBioscience, unless otherwise stated. The mAbs used for immunofluorescence staining of frozen sections were anti-RANKL (IK22-5), anti-RANK (LOB14-8; GeneTex), PE-conjugated anti-B220 (RA3-6B2), biotinylated GL7 (for detection of activated germinal center B cells), and allophycocyanin-conjugated

anti-Thy1.2 (53-2.1; BD Biosciences). The rat mAb NKM 16-2-4 specific for mouse M cells was purified from hybridoma supernatant and labeled with FITC (35). A purified rat IgG2a isotype control mAb (BD Biosciences) was used as a control for staining of frozen tissue sections with the rat IgG2a anti-RANKL and anti-RANK mAbs. Biotinylated polyclonal goat anti-rat IgG (BD Biosciences) was used as a secondary reagent for detection of most unconjugated rat primary mAb. Rhodamine-UEA-I was purchased from Vector Laboratories. The anti-RANKL Ab (IK22-5) used for in vivo RANKL neutralization experiments was prepared as described previously (36). Mice were treated with 250 μg of IK22–5 or a purified functional grade control rat IgG2a mAb (eBioscience) i.p. every 2 days.

Immunofluorescence staining of frozen sections

Frozen sections of PP and adjacent intestinal tissue were cut on a cryostat and prepared for Ab staining experiments as previously described (29). The sections were washed in PBS and blocked in TNB buffer (PerkinElmer Life Sciences). Abs diluted in TNB buffer were applied for 1 h at room temperature or overnight at 4°C. Biotinylated primary mAbs were detected using streptavidin-conjugated peroxidase followed by FITC-tyramide from a tyramide signal amplification kit (PerkinElmer Life Sciences). Unconjugated primary rat mAbs were detected by a combination of biotinylated polyclonal goat-anti-rat IgG (BD Biosciences) followed by streptavidin-peroxidase and FITC-tyramide. DAPI (Sigma-Aldrich) at 10 ng/ml was used as a nuclear counterstain. The slides were mounted in ProLong antifade reagent (Invitrogen). Images were acquired using a Nikon 80i fluorescence microscope and edited when necessary with Photoshop (Adobe Systems).

Electron microscopy

Mice were perfusion fixed using 2.5% glutaraldehyde solution in 0.1 M cacodylate buffer. For transmission electron microscopy, individual PP were isolated, bisected through the center of the domes, and embedded in Epon resin. Thin sections from the PP domes of control and RANKL null mice were examined using a JEOL JEM-1210 microscope. For scanning electron microscopy, small intestinal villi were subjected to critical point drying, sputter coated with gold, and examined on a Topcon DS-130F field emission scanning electron microscope.

Whole mount staining of small intestine tissue for detection of UEA-I$^+$ M cells

For detection of M cells in PP, individual PP were excised and vortex mixed in 0.5% Tween 20-PBS followed by a shaking incubation with 100 μg/ml DNase for 20 min at 37°C to promote dissociation of mucus from the epithelial layer. The PP were blocked with TNB buffer for 15 min at 4°C, and stained with rhodamine-UEA-I in TNB for 40 min at 4°C. Each stained PP was mounted under a 20 mm × 20 mm coverslip in 100 μl PBS. A count of UEA-I$^+$ M cells was done for the PP follicle with the most M cells. This method resulted in some degree of underestimation of the full extent of M cell depletion in RANKL null mice because often only one of several PP follicles had any M cells in the mutant mice, while all the follicles in wild-type PP typically had a comparable number of M cells. To examine small intestine tissue for the presence of villous M cells, thin strips of tissue were cut and stained with rhodamine UEA-I as described above for PP. Villi with M cells on their surface were classified as showing a dense or diffuse pattern of villous M cells using criteria based on the initial description of these patterns by Jang et al. (9). Specifically, villi with one or more clusters of M cells in which 75% or more of the area within the cluster was occupied with M cells were considered to have a dense distribution of villous M cells. Villi with at least one characteristic UEA-I$^+$ M cell on the surface, but not meeting the dense distribution criteria, were considered to have a diffuse distribution.

Quantitative analysis of fluorescent bead and bacteria uptake by M cells

Analysis of the degree of bead uptake from loops containing PP was done by threshold analysis using ImageJ v1.36b software (http://rsb.info.nih.gov/ij/). Images of the fluorescent beads found within sections of individual PP follicles were saved as 8-bit grayscale images and then converted to binary images showing the beads by thresholding at a grayscale cutoff point of 75 of 255. The percentage of the pixels with a signal intensity that exceeded this cutoff was calculated for the area occupied by each PP follicle. Analysis of the bead uptake from loops lacking PP was done by a similar approach. Images of sections showing just the fluorescent beads within epithelial cells and the villi were thresholded at a grayscale cutoff point of 55 out of 255. Images of the DAPI-stained nuclei in the same field acquired in a separate channel were thresholded at a cutoff point of 70. The extent of bead uptake was expressed as the ratio of pixels with fluorescent beads to pixels with DAPI after normalization to a mean value of 1.0 for loops from mice not treated with RANKL. Analysis of fluorescent bacteria uptake from loops lacking PP was done by counting of the number of organisms present in sections of villi showing the villus from its base to the tip. The data were reported as the percentage of villi that included at least one organism and the average number of organisms per villus. The latter statistic was normalized to a value of 1.0 for loops from mice not treated with RANKL.

ELISA for measurement of fecal IgA

Fecal pellet samples were collected and extracted by making a 1/10 suspension (w/v) with PBS. After the suspension was vortexed and spun for 10 min at 12,000 × *g*, the supernatant was stored at −70°C. Polyclonal goat anti-mouse IgA Ab (Southern Biotechnology) was used as a capture Ab. The bound mouse IgA was detected with peroxidase-labeled goat anti-mouse IgA Ab (Southern Biotechnology) using TMB (BD Biosciences) as the peroxidase substrate. A mouse IgA,κ isotype control mAb (BD Biosciences) was used to establish a standard curve.

Statistical analysis

Differences between the mean values for groups were analyzed by either two-tailed ANOVA with Tukey correction (for multiple groups), two-tailed Student's *t* test, or two-tailed Mann-Whitney *U* test as calculated using Prism (GraphPad Software). Differences in the frequency of bacterial uptake into villi were analyzed by Fisher's exact test and also calculated with Prism. A *p*-value of <0.01 was considered significant.

Results

UEA-I$^+$ M cells are dramatically decreased in the FAE of PP from RANKL null mice

M cells in mouse PP can be detected using the UEA-I lectin specific for α(1, 2)-fucose linkages. In wild-type mice, whole mount microscopy of PP follicles revealed an average of over 100 radially arranged UEA-I$^+$ M cells that extended from the edges of the follicles toward the central subepithelial dome area. In contrast, UEA-I$^+$ M cells were either completely absent or very sparsely represented in individual follicles from the PP RANKL null mice (Fig. 1*A*). The few remaining UEA-I$^+$ cells in RANKL null mice were mostly located at the periphery of the follicle and did not have the usual polygonal shape of normal M cells, features suggesting these remaining M cells were abnormal. The loss of M cells in PP from RANKL null mice was confirmed by staining PP sections with NKM 16–2-4 (supplementary Fig. S1),[4] a recently described rat mAb that is more selective than UEA-I for the specific α(1, 2)-fucose moiety characteristically displayed by mouse M cells (35). Cells with the defining ultrastructural features of M cells by transmission electron microscopy (i.e., presence of intraepithelial pockets and blunting of the apical microvilli in comparison to normal enterocytes) were readily apparent in the FAE from control mice, but absent from the FAE of RANKL null mice (Fig. 1*B*). Although the number of UEA-I$^+$ M cells was significantly decreased in all PP examined from RANKL null mice, a proximal to distal gradient in the number of UEA-I$^+$ cells per dome was observed in RANKL null mice that was not seen in wild-type mice (Fig. 1*C*). UEA-I$^+$ M cells were almost completely absent in the most proximal PP from RANKL null mice, and progressively increased in more distal PP. In RANKL null mice, the highest number of residual UEA-I$^+$ cells was consistently detected in the most distal ileal PP. Taking into account the decreases in RANKL null mice in the number of PP, the number of follicles in each PP, and the number of M cells per follicle, loss of RANKL is associated with a 73-fold overall depletion of UEA-I$^+$ M cells. This extent of loss of M cells is roughly 10-fold greater than the losses we observed in both μMT B cell deficient mice and CCR6 deficient mice

[4] The online version of this article contains supplemental material.

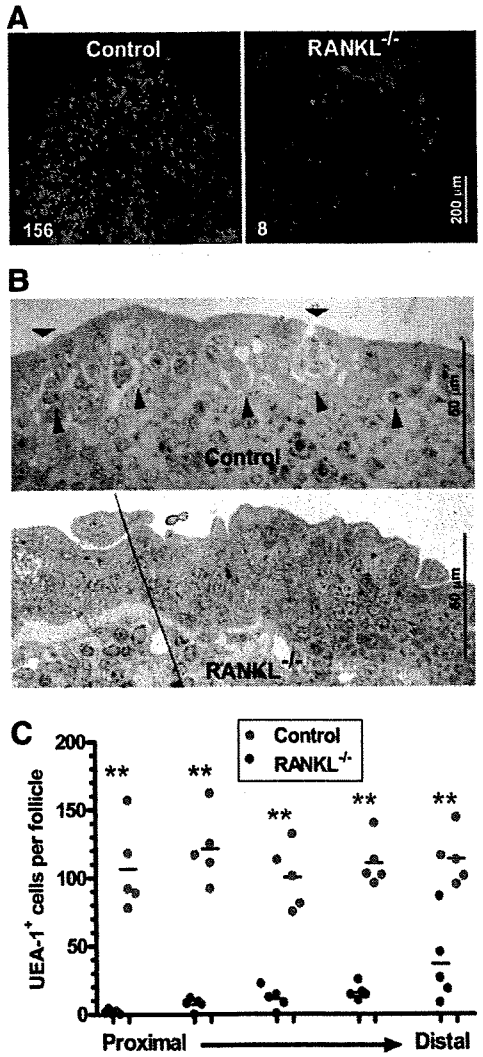

FIGURE 1. PP of RANKL null mice contain very few M cells. *A*, UEA-I staining reveals far fewer M cells in a representative follicle from a PP from a (C57BL/6 × BALB/c)F_1 RANKL null compared with a wild-type control PP. The number of M cells counted in the follicle is indicated in the lower left hand corner. The follicles shown are from the middle portion of the small intestine. Scale bar, 200 μm. *B*, FAE of a (C57BL/6 × BALB/c)F_1 RANKL null mice showed a lack of characteristic M cell features by transmission electron microscopy. The long arrowheads indicate intraepithelial pockets within the M cells of the wild-type FAE. The short arrowheads point to the shorter microvilli found on the apical surface of M cells. Scale bars, 50 μm. *C*, Scatter plot summarizing frequency of UEA-I^+ M cells in individual PP follicles from mixed background RANKL null and control mice (n = 5 mice for both groups). All PP examined were assigned to 1 of 5 groups based on proximal to distal position. **, $p \leq 0.001$ compared with control mice by ANOVA.

(data not shown), strains of mutant mice previously shown to have a significant reduction in the number of M cells (37, 38).

UEA-I^+ M cells can be restored in RANKL null mice by treatment with exogenous RANKL

To determine whether the deficiency of M cells in the FAE of RANKL null PP could be restored by replacement of RANKL, RANKL null mice were injected i.p. for 7 consecutive days with 250 μg per day of either recombinant GST-RANKL fusion protein or recombinant GST as a control. On day 7, the PP follicles of RANKL null mice treated with GST-RANKL had a near normal number of UEA-I^+ M cells distributed in the typical radial pattern, while GST-treated mice remained profoundly M cell deficient (Fig. 2*A*). Daily treatment of RANKL null mice with rGST-RANKL for shorter intervals demonstrated that day 5 was the first time point at which the number of UEA-I^+ M cells was significantly increased over untreated RANKL null mice (Fig. 2*B*).

RANKL null mice have a defect in the uptake of 200 nm fluorescent beads into PP follicles that is corrected by administration of RANKL

Although UEA-I is a useful immunohistochemical marker of mouse M cells, this method of identification does not detect M cells based on their specialized ability to take up particulate Ags from the lumen and transport them to meet APC in the intraepithelial pockets. Measuring uptake of fluorescent nanoparticles injected into loops of small intestine is a method that directly assesses M cell function in the FAE of PP (33, 34). Frozen sections of PP in isolated loops of small intestine from RANKL null mice and RANKL null mice treated with GST-RANKL or GST (as a control) were compared at 90 min after injection of fluorescent 200 nm nanoparticles into the loops. In the GST-RANKL-treated mice, more UEA-I^+ M cells were present and some of these cells contained multiple fluorescent beads (Fig. 2*C*). Beads that had already passed through the epithelial layer to reach the PP follicle were observed in APC in the vicinity of the subepithelial dome or deeper in the B cell follicle. Image analysis was used to quantify the magnitude of bead uptake in the GST-RANKL reconstituted mice and controls (Fig. 2*D*). Untreated RANKL null mice or those treated with GST had over 10-fold less uptake of beads than control wild-type mice. GST-RANKL treatment for 7 days restored bead uptake to near wild-type levels.

Systemic administration of RANKL also leads to widespread induction of villous M cells

In the course of treating RANKL null mice with GST-RANKL and evaluating the reconstitution of M cells in PP, we noticed that the number of UEA-I^+ cells present on small intestinal villi was also increased. This effect of RANKL treatment was further evaluated in BALB/c mice, in which <10% of small intestinal villi have any villous M cells at baseline, with most of these rare villous M cells arranged in a diffuse pattern. Treatment with systemic GST-RANKL i.p. for 4 consecutive days induced substantial increase in the number of UEA-I^+ cells with the features of M cells on the surface of the villi (Fig. 3*A*). Induction of an increased number of villous M cells began by 24 h after the first injection of GST-RANKL; 4 days after the start of RANKL treatment all small intestinal villi had at least some UEA-I^+ cells present, with 70% of villi showing a diffuse pattern and the remaining 30% exhibiting a dense pattern (Fig. 3*B*). In villi showing a diffuse pattern of villous M cells, UEA-I^+ cells represented ~3% of the total number of cells with DAPI$^+$ nuclei. Scanning electron microscopy of villi from RANKL-treated mice revealed slightly sunken cells with the characteristic stubby microvilli characteristic of M cells (Fig. 3*C*).

RANKL-induced villous M cells are functional M cells capable of taking up 200 nm beads and enteric bacteria

To determine whether the villous M cells induced by systemic RANKL treatment were capable of increased transport of particulate Ags across the epithelium, mice were treated with s.c. injections of GST-RANKL or GST as a control for 4 consecutive days and gavaged with 200 nm diameter fluorescent nanoparticles at the same time as the last two RANKL injections. Small intestinal segments from these mice were excised 24 h after the second dose of beads and frozen sections cut to identify beads that had been taken

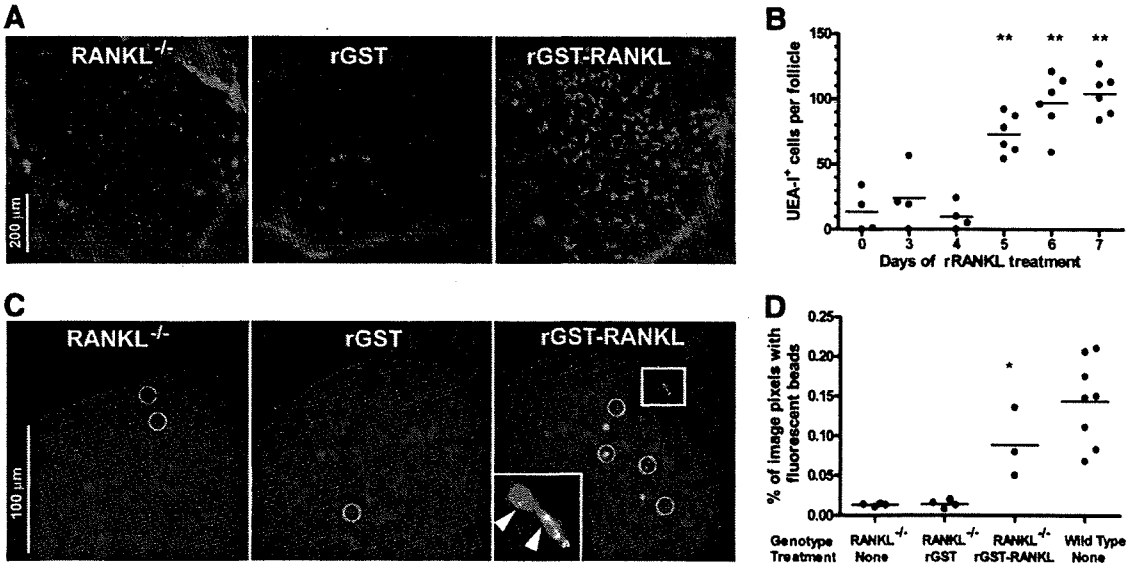

FIGURE 2. Administration of rRANKL to RANKL null mice restores PP M cells. *A*, (C57BL/6 × BALB/c)F_1 RANKL null mice were treated i.p. for 7 days with 250 µg/day of GST-RANKL or GST as a control. UEA-I staining of representative follicles from the distal small intestine shows restoration of the normal number and pattern of UEA-I^+ M cells by GST-RANKL, but not by GST. Scale bar, 200 µm. *B*, Reconstitution of UEA-I^+ M cells requires 5 days of treatment with GST-RANKL. The results are based on three to six mixed background mice at each time point and include data from all PP except the most distal PP. **, $p \leq 0.001$ compared with untreated mice by ANOVA. *C*, Uptake of 200-nm diameter fluorescent beads from isolated small intestinal loops into PP of mixed background RANKL null mice 90 min after bead injection is restored to near wild-type levels by prior treatment with GST-RANKL for 5 days. Merged images of bead fluorescence and DAPI fluorescence from frozen sections of PP are shown with the white circles indicating the location of individual beads or clusters of beads. The inset shows a magnified image of the boxed area additionally merged with the rhodamine-UEA-I signal to show that the clusters of fluorescent beads (indicated by arrowheads) within two adjacent UEA-I^+ M cells on the surface of the FAE. Scale bar, 100 µm. *D*, Summary scatter plot showing that GST-RANKL treatment reconstitutes uptake of fluorescent beads as assessed by image analysis of the percentage of pixels containing green fluorescent beads within the area of the PP follicles. *, $p < 0.01$ compared with untreated RANKL-null mice by ANOVA.

up into the lamina propria by M cells. Bead uptake was readily apparent in M cells and within the villi of the RANKL-treated mice, but barely evident in the control untreated mice (Fig. 4*A*). Uptake of fluorescent beads was increased by an average of 74-fold over the baseline of untreated mice as a result of RANKL-induction of villous M cells (Fig. 4*B*). To test whether the RANKL-induced villous M cells were also capable of enhanced uptake of enteric bacteria, isolated segments of small intestine lacking any PP from mice treated with GST-RANKL or GST for 4 days were injected with fluorescently labeled paraformaldehyde-fixed enteric bacteria. Sections of the intestinal wall taken 2 h after the introduction of the bacteria revealed substantially enhanced uptake of both *Salmonella enterica* serovar Typhimurium (35-fold) and *Yersinia enterocolitica* (46-fold) as a consequence of villous M cell induction by RANKL (Fig. 4, *C* and *D*).

Neutralizing Ab to RANKL reproduces the M cell deficiency observed in RANKL null mice

Some of the developmental defects in RANKL null mice, such as the total absence of lymph nodes, cannot be corrected by simply injecting the mice with the absent cytokine as adults. This raises the issue of whether the M cell deficit observed in PP from RANKL null mice might be a byproduct of early developmental alterations in the PP of these mice. To address this issue, wild-type BALB/c mice were treated i.p. with a neutralizing anti-RANKL Ab to determine whether acute blockade of RANKL-RANK signaling would lead to loss of PP M cells. Mice were treated i.p. with 250 µg of the IK22–5 rat anti-mouse RANKL mAb every 2 days, a dose previously shown to block the activity of RANKL in vivo (36). The number of M cells in the PP follicles was evaluated after various lengths of treatment by both UEA-I staining and by uptake of fluorescent 200 nm beads from isolated small intestinal loops. After 8 days of Ab treatment, the number of M cells present in the PP and the degree of uptake of fluorescent beads by PP in isolated loops were both dramatically decreased compared with untreated mice or mice treated with an isotype control IgG2a mAb (Fig. 5, *A–C*). Analysis of the kinetics of the anti-RANKL effects showed that the number of UEA-I^+ M cells dropped precipitously between 2 and 4 days, and declined further between 4 and 8 days (Fig. 5*D*).

Epithelial cells in the small intestine express RANK

RANK is expressed by multiple cell types including osteoclasts, DCs, mammary epithelial cells, and thymic epithelial cells. Because our experiments with RANKL null mice and neutralizing anti-RANKL Ab showed that RANKL is essential for normal M cell development within the FAE, we used immunohistochemical staining with anti-RANK Abs to determine what cells in the vicinity of PP expressed the RANK. Staining for RANK was observed on the apical and basolateral aspects of epithelial cells in the FAE, and was also detected on villous and crypt epithelial cells (Fig. 6). Serial sections of the same PP showed that RANKL expression was restricted to stromal cells concentrated beneath the FAE as previously shown (29). These results suggest that RANKL exerts its effects on M cell differentiation through short-range delivery from the stromal cells to the FAE on the other side of the basement membrane.

RANKL null mice exhibit decreased PP germinal center formation and fecal IgA production

PP were previously reported to be smaller than normal in two independently derived strains of RANKL null mice (22, 23), but other aspects of PP function were not examined in the initial reports. We asked whether the loss of M cell function in RANKL null mice was associated with impaired B cell responses to Ags

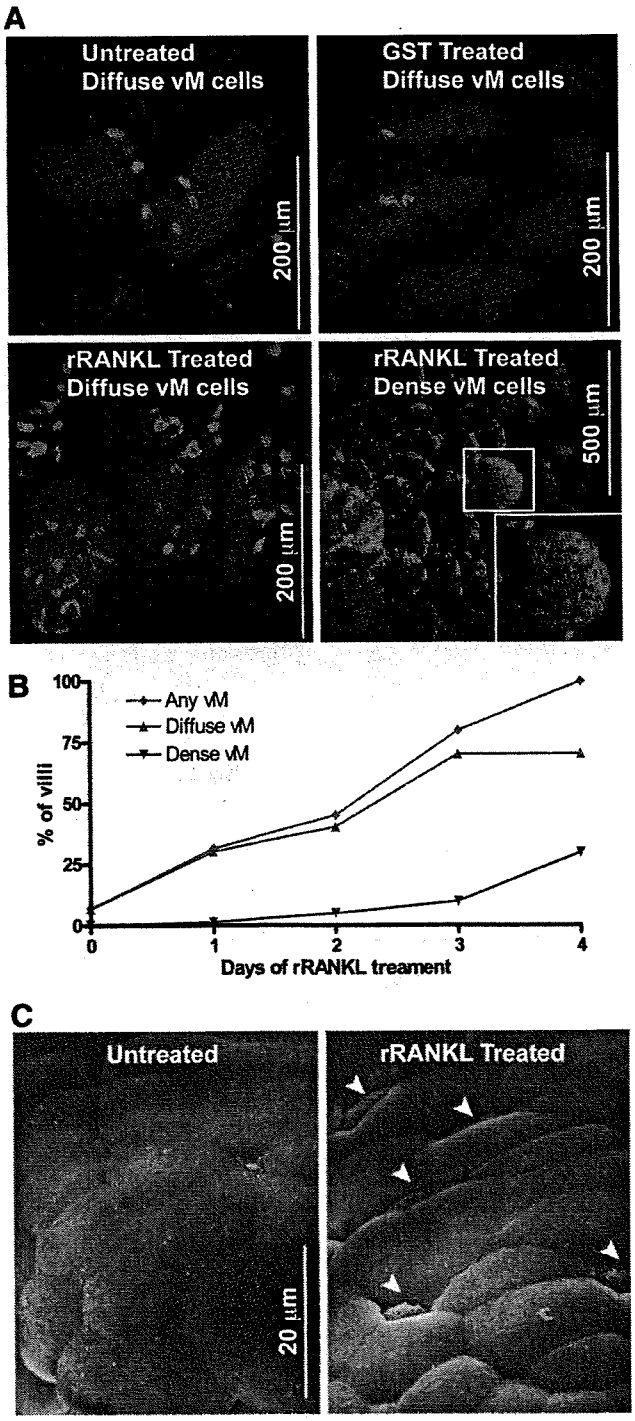

FIGURE 3. Administration of rRANKL induces development of villous M cells on all small intestinal villi. *A*, Whole mount staining of villous M cells in untreated BALB/c mice and mice treated for 4 days with GST-RANKL or GST (an initial injection of 50 μg i.p. followed by 100 μg s.c. every 24 h) with rhodamine-UEA-I and DAPI. In untreated mice, a few villous M cells in a diffuse pattern are present on occasional villi. GST-RANKL treatment leads to an increased fraction of the villi having M cells and an increase in the number of M cells per villus. The fraction of villi exhibiting both the diffuse and dense patterns of villous M cell distribution increases after GST-RANKL. Scale bars, 200 μm and 500 μm. *B*, Summary graph showing kinetics of induction of villous M cells in the diffuse and dense patterns of distribution following GST-RANKL administration. *C*, Scanning electron microscopy reveals the presence of cells with a depressed surface and attenuated and blunted microvilli characteristic of M cells.

internalized from the intestinal lumen. We compared the frequency and extent of germinal center development in PP from RANKL null mice and littermate controls using an Ab (GL7) that preferentially binds activated germinal center B cells. Compared with PP from controls, PP from RANKL null mice at 10 to 12 wk of age exhibited a smaller percentage of germinal centers containing $GL7^+$ cells in the B cell zones and a relative expansion of the T cell zones (Fig. 7*A*). This finding suggested that the production of secretory IgA might also be impaired in RANKL null mice. Fecal IgA concentrations in mice from 4 to 12 wk of age were consistently decreased in RANKL null mice compared with littermate controls (Fig. 7*B*).

Discussion

Ag-sampling M cells have been described in both mammalian and avian species as part of the FAE covering the organized lymphoid structures of the respiratory and digestive tract (3, 39, 40). However, the specific signals and signaling pathways that trigger the differentiation of these M cells from precursor cells located in the stem cell zone of the crypts or from the enterocytes on the surface of the FAE remain to be identified (12). Some clues have emerged from analysis of strains of mutant mice created by gene-targeting that retain PP but exhibit decreased numbers of M cells in these PP. Specifically, B cell-deficient mice such as μMT mice exhibit significantly reduced numbers of M cells in PP (37). Additional support for a role of B cells in promoting M cell development has come from in vitro studies in which coculture of freshly isolated B lymphocyte or B lymphocyte lines with model intestinal epithelial cell lines cultured on semipermeable supports promoted the development of M cell-like features by the epithelial cells, including transcytosis of particulate Ags (11, 41). However, neither in vivo analysis of PP from B cell-deficient mice or experiments based on the in vitro M cell differentiation system have elucidated a specific mechanism by which B cells promote differentiation of M cells in the FAE.

RANKL emerged as a cytokine with a potential role in the differentiation of the FAE and M cells as a result of experiments demonstrating RANKL expression on stromal cells located immediately beneath the FAE in ILF and PP (29). To determine whether PP were functionally compromised in the absence of RANKL, we characterized the PP of RANKL null mice. Staining of PP from RANKL null mice with the UEA-I lectin reactive with murine M cells revealed a profound depletion in $UEA\text{-}I^+$ cells compared with wild-type mice. Taking into account all of the factors that contribute to the total number of M cells within small intestinal PP (i.e., number of PP, number of follicles per PP, number of M cells per follicle), we found that RANKL null mice have <2% of the number of $UEA\text{-}I^+$ M cells found in wild-type mice. Although the UEA-I lectin was the primary immunohistochemical reagent we used to establish that RANKL null mice are deficient in M cells, we have used several independent means of confirming this deficiency in M cells including functional measurements of M cell activity using uptake of fluorescent nanoparticles and bacteria, transmission electron microscopy, and immunostaining with the NKM 16-2-4 mAb specific for mouse M cells.

RANKL acting through its specific receptor (RANK) plays an important developmental role in multiple tissues. The most striking and best-studied of the deficits in RANKL null mice are the absence of any lymph nodes and the failure of osteoclast development, leading to osteopetrosis and a malformed skeleton. One potential explanation of the loss of M cells we observed in PP from RANKL null mice is an early developmental defect in PP development that permanently compromises the capacity of the FAE to generate conventional M cells. Two types of experiments were

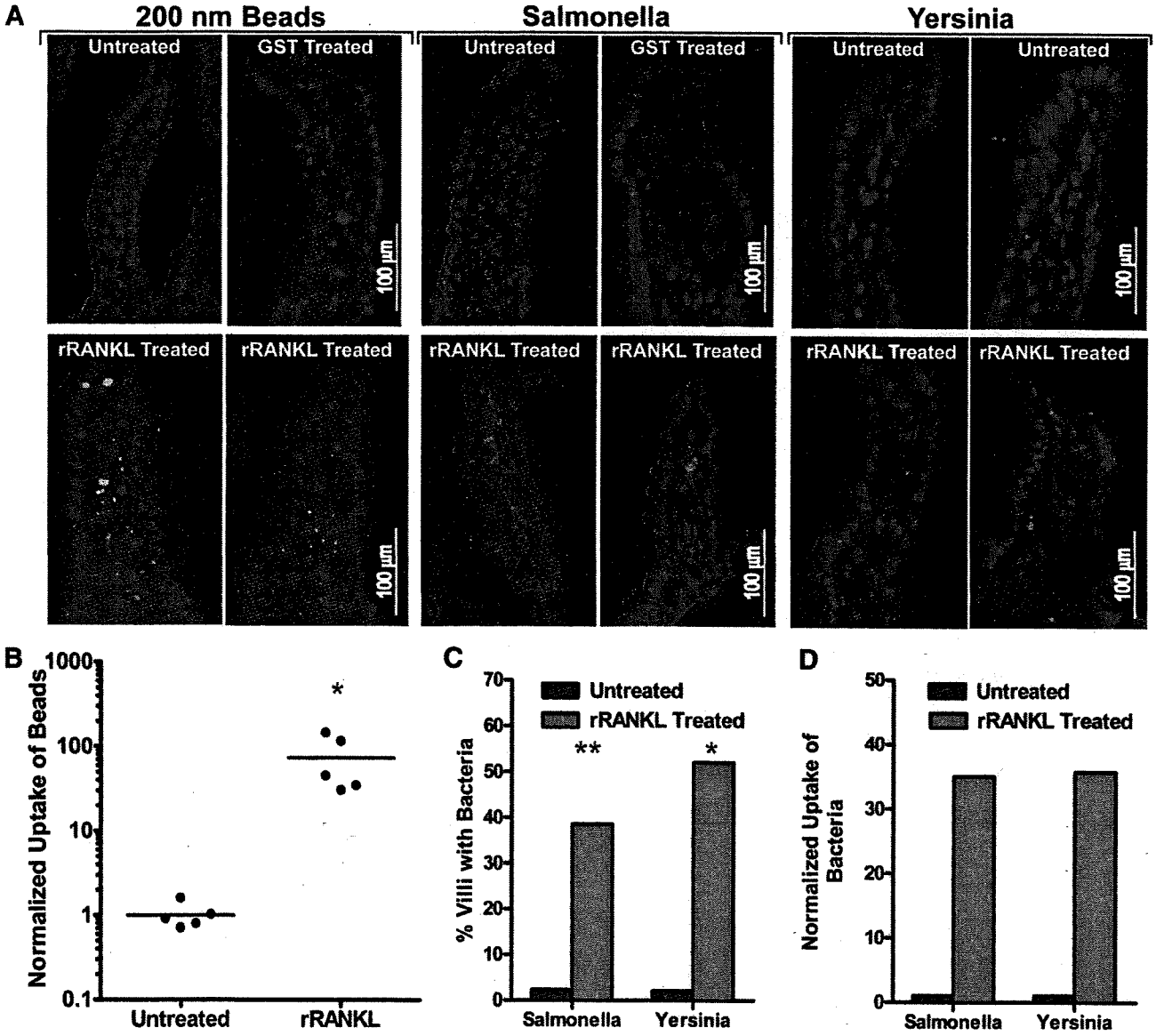

FIGURE 4. RANKL-induced villous M cells are functional for bead and bacteria uptake from the intestinal lumen. *A*, Wild-type (C57BL/6 × BALB/c)F_1 mice were treated with 100 μg of GST-RANKL or GST s.c. once a day for 4 consecutive days. On the last two days of injections, the mice and untreated controls also received 1×10^{11} 200 nm fluorescent beads by gavage. One day after the last dose of GST-RANKL or GST, segments of small intestine were harvested and sectioned to check for the presence of green fluorescent beads. Alternatively, isolated small intestinal loops were prepared in anesthetized mice treated for 4 days with RANKL or GST and untreated controls and these loops were injected with paraformaldehyde-fixed *Salmonella enterica* serovar Typhimurium expressing DsRed-Express or *Yersinia enterocolitica* labeled with Alexa546. After a 2-h incubation, the tissue was harvested for frozen sections. The merged images show representative villi with DAPI-positive nuclei and either green fluorescent beads or red fluorescent bacteria within the villi. *B*, Uptake of beads was quantitated by image analysis and normalized so that the average uptake in untreated controls was 1.0. *, $p < 0.01$ by Mann-Whitney *U* test. *C*, The percentage of villi containing at least one bacterial organism was substantially increased in RANKL-treated mice. **, $p \leq 0.001$; *, $p < 0.01$ (both by Fisher's exact test). *D*, Uptake of bacteria was quantitated by counting individual bacteria within villi. The mean number of bacteria found per villus was normalized to a value of 1.0 for the untreated controls.

done to test this possibility. First, we examined whether the M cell defect was reversible if a source of exogenous recombinant RANKL was provided. Daily injections of GST-RANKL given for 5 or more days provided a nearly complete reconstitution of the number of M cells per PP follicle. Second, we used neutralizing mAb to RANKL to test whether acute depletion of RANKL in adult wild-type mice would also cause loss of M cells. After 4 days of anti-RANKL treatment to inhibit normal RANKL-RANK interactions, the number of UEA-1^+ M cells in each PP follicle plunged to levels approaching those in the RANKL null mice. Thus, production of RANKL must be sustained in the adult PP to permit the continued production and/or survival of M cells.

RANK is expressed on multiple cell types including osteoclasts and their precursors, DCs, endothelial cells, mTEC, and mammary epithelial cells. The simplest model to explain the observed effects of RANKL on M cell differentiation is to propose that RANKL derived from the subepithelial dome stromal cells in the PP acts in a paracrine fashion on the adjacent epithelial cells of the FAE. Because RANKL is a type II membrane protein that is synthesized in a transmembrane form, cleavage by metalloproteases is needed

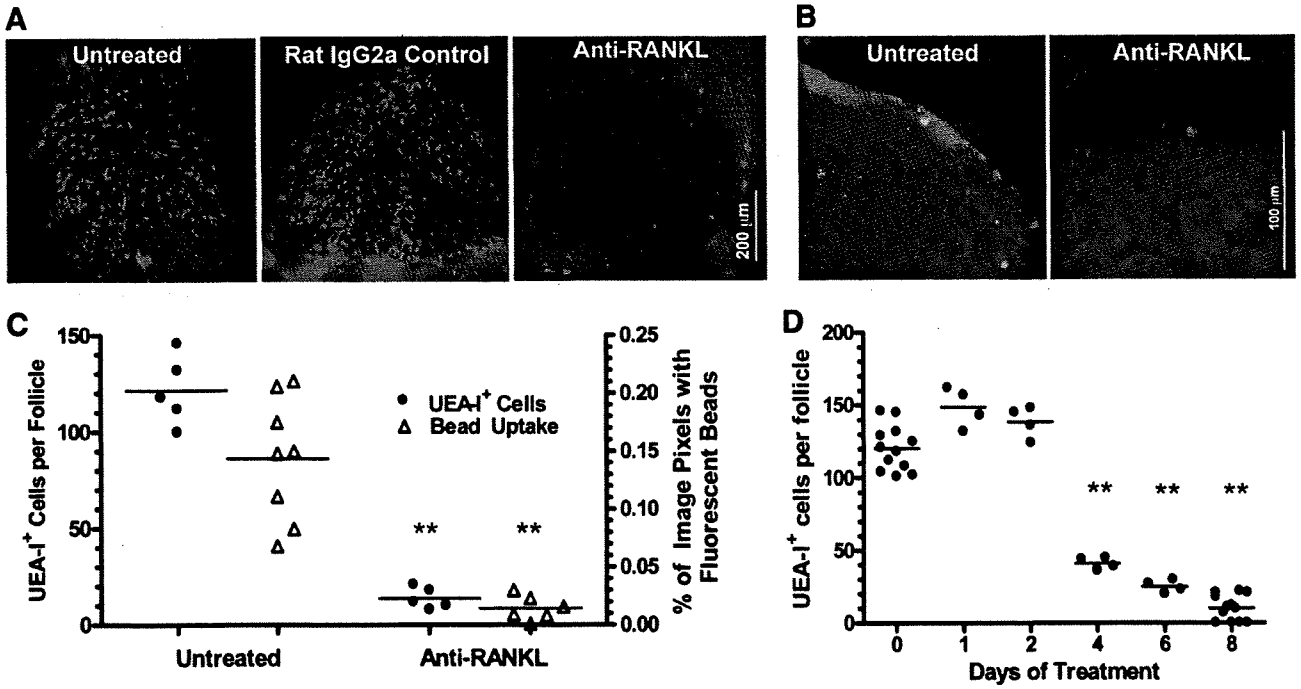

FIGURE 5. Treatment of wild-type mice with neutralizing anti-RANKL leads to loss of PP M cells. *A* and *B*, BALB/c mice were treated i.p. with 250 μg of IKK22–5 mAb or an isotype control rat IgG2a mAb on days 0, 2, 4, and 6. On day 8, isolated bowel loops containing PP were injected with fluorescent beads and the mice euthanized after 90 min. Anti-RANKL treatment led to loss of UEA-I$^+$ M cells detected by whole mount staining (*A*) and a decrease in the uptake of fluorescent beads detected on frozen sections of PP from the bead-injected loops (*B*). Scale bar, 200 μm in *A* and 100 μm in *B*. *C*, Summary of data from all PP analyzed in *A* and *B* for UEA-I$^+$ cells and fluorescent bead uptake. *D*, Anti-RANKL-induced loss of UEA-I$^+$ M cells detected by whole mount staining begins by 4 days after start of Ab treatment. ** in *C* and *D* indicates $p < 0.001$ compared with untreated mice by *t* test (*C*) or ANOVA (*D*).

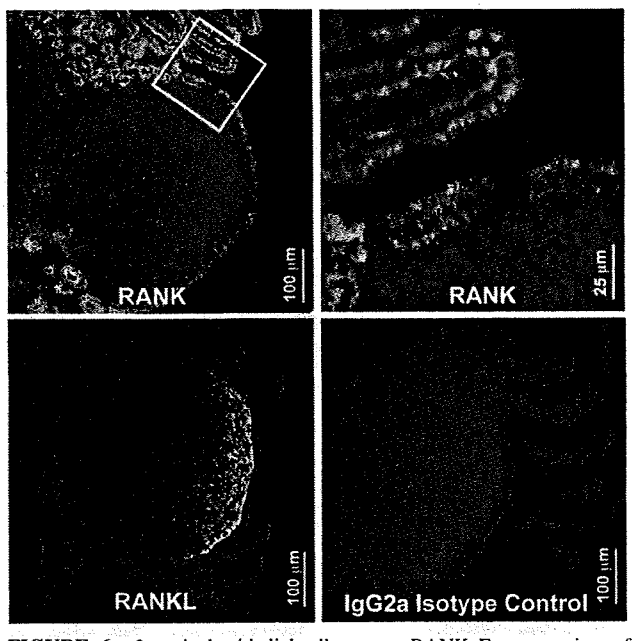

FIGURE 6. Intestinal epithelial cells express RANK. Frozen sections of a PP from a single wild-type BALB/c mouse were stained with rat mAbs to mouse RANK (*A* and *B*), mouse RANKL (*C*), or an isotype control rat IgG2a mAb (*D*), followed by a biotinylated secondary Ab, streptavidin-peroxidase, and FITC-tyramide plus DAPI as a counterstain. *A*, RANK expression is localized to epithelial cells in the FAE and on the adjacent villi. Scale bar, 100 μm. *B*, Higher magnification of boxed area from *A* showing that RANK is present on both the apical and basolateral surfaces of the FAE. Scale bar, 250 μm. *C*, Reticular stromal cells concentrated immediately beneath the epithelial layer are the only cells on which RANKL is detected. Scale bar, 200 μm. *D*, No staining is observed with the rat IgG2a isotype control.

to generate a soluble form of the cytokine (17, 18). We favor the hypothesis that RANKL is acting directly through RANK on enterocytes because immunohistochemical staining of small intestinal tissue including a PP showed that the bulk of the RANK staining is localized to the epithelium, with roughly equivalent levels of RANK on the FAE and villous epithelium. Gene expression profiling studies comparing flow sorted PP M cells and villous enterocytes revealed that both of these intestinal epithelial cell types express mRNA for RANK (35) (gene expression data for RANK archived in NCBI Gene Expression Omnibus under accession number GSE7838; http://www.ncbi.nlm.nih.gov/geo/query/acc.cgi?acc=GSE7838). Although the induction of M cells by RANKL appears to be mediated by direct action of RANKL on RANK-expressing epithelial cells, other cell types in the small intestine are known to express RANK and respond to RANKL. For example, RANKL was shown to act on PP DC to enhance IL-10 production (42). In addition, Ab-mediated neutralization of RANKL in a transfer model of colitis resulted in decreased regulatory T cell activity, suggesting that RANKL-RANK signaling contributes to the normal function of regulatory T cells (43).

The capacity of soluble recombinant RANKL injected systemically to induce the appearance of M cells on all small intestinal villi provides further insights into the mechanism of action of RANKL. RANK-expressing epithelial precursor cells located in both dome-associated crypts next to PP follicles and in standard small intestinal crypts have the potential to differentiate into M cells if exposed to sufficient stimulation with RANKL. RANKL-induced villous M cells have most of the same features as PP M cells, including reactivity with UEA-I, stubby surface microvilli observed by scanning electron microscopy, and most importantly the capacity for constitutive uptake of particulate Ags. Under normal conditions, M cell development is primarily restricted (other than a small number of scattered villous M cells) to the organized

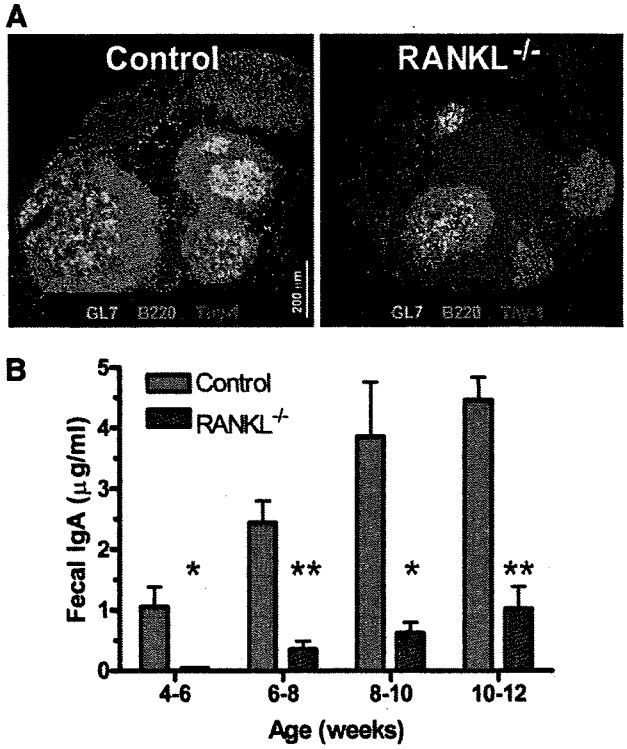

FIGURE 7. RANKL$^{-/-}$ mice have fewer germinal centers in their PP follicles and lower levels of fecal IgA. *A*, RANKL$^{-/-}$ PP on a mixed C57BL/6 and BALB/c background have fewer and less developed germinal centers identified by GL7$^+$ cells than control PP. *B*, Fecal IgA concentrations (mean ± SD) measured by ELISA were consistently decreased in RANKL$^{-/-}$ mice compared with littermate controls based on analysis of samples from 5 to 16 mice of each genotype in each age range tested. *, $p < 0.01$; **, $p < 0.001$ (compared with control mice by *t* test).

lymphoid tissues of the small intestine (i.e., PP and ILF) because constitutive expression of RANKL is restricted to subepithelial stromal cells at these sites. When the spatial restriction of RANKL availability in the small intestine is bypassed by systemic injection, RANKL is able to trigger M cell differentiation in a fraction of epithelial precursors in both dome-associated crypts adjacent to organized lymphoid tissues and normal crypts.

Although our results identify RANKL as a key cytokine signal involved in inducing the differentiation of M cells from precursors in the FAE, we consistently observed a trace number of residual UEA-I$^+$ M cells in a few of the PP follicles in RANKL null mice. Our results fit best with a model that postulates that there are additional signals besides RANKL that contribute to the development of M cells. We found that the most distal PP in RANKL null mice was invariably the PP with the largest number of residual M cells per follicle, suggesting that an increased density of luminal commensal bacteria can accentuate the extent of M cell differentiation locally in situations in which loss of an M cell-inducing factor results in a global decrease in M cell differentiation. One of the other signals capable of promoting M cell development may be contributed by local B cells in the PP, because absence of mature B cells also leads to depletion of PP M cells (37), although the degree of M cell deficit is far less pronounced. Exogenous administration of GST-RANKL to B cell deficient $J_H^{-/-}$ mice does not increase the number of PP M cells (our unpublished observations), indicating that the contribution of B cells to the development of M cells does not involve simply providing RANKL. Given that TNF family members are known to have overlapping and partially redundant functions in other developmental contexts (e.g., the known contributions of lymphotoxin $\alpha_1\beta_2$, RANKL, and TNF-α to the normal formation and organization of secondary lymphoid structures) (44), other TNF family members may contribute to the induction of M cell differentiation and account for the low level of residual M cell formation in the absence of RANKL. Cooperation of RANKL with the TNF family member CD40L has recently been established for the induction of mTEC differentiation (24, 25). RANKL is the most critical TNF family member in inducing normal mTEC differentiation during embryonic development of the thymus, with CD40L playing a complementary role in the postnatal thymus (24). Interesting parallels exist between the role of RANKL in inducing differentiation of UEA-I$^+$ M cells in the FAE of PP and its role in inducing the differentiation of UEA-I$^+$ mTEC in the thymus. The RANKL-induced mTECs are critical for establishment of central T cell tolerance, while RANKL-induced M cells contribute to the establishment of peripheral T cell tolerance to bacterial Ags at mucosal surfaces normally colonized by commensal bacteria.

The identification of RANKL as a key switch factor that can elicit M cell development by intestinal epithelial precursors has the potential to yield valuable translational applications in the areas of mucosal vaccine development and oral tolerance induction. Specifically targeting orally administered Ags to M cells using either mAbs to M cell surface receptors, lectins, or bacterial adhesins specific for M cells remains an active area in the development of vaccines for oral delivery (45, 46). Combining Ab-mediated M cell targeting of Ag with a strong mucosal adjuvant (e.g., cholera toxin) already shows promise as a strategy for the establishment of both mucosal and systemic immunity to vaccine Ags (47). The efficacy of such approaches may be boosted if preceded by systemic or ideally local delivery of exogenous RANKL aimed at increasing the frequency of human M cells in the PP FAE and particularly in the villous epithelium to supraphysiologic levels, thereby increasing the efficiency of delivery of M cell-targeted vaccines administered at mucosal surfaces.

Acknowledgments

We thank Dr. Max Cooper for valuable suggestions and Dr. Tim Denning for comments on the manuscript. We also thank Dr. Yongwon Choi for providing us with RANKL knockout mice, Katy Gray in Dr. Sam Speck's laboratory for help obtaining breeder pairs of μMT mice, and Jeannette Taylor from the Robert P. Apkarian Integrated Electron Microscopy Core for expert technical assistance with electron microscopy.

Disclosures

The authors have no financial conflict of interest.

References

1. Fagarasan, S., and T. Honjo. 2004. Regulation of IgA synthesis at mucosal surfaces. *Curr. Opin. Immunol.* 16: 277–283.
2. Iweala, O. I., and C. R. Nagler. 2006. Immune privilege in the gut: the establishment and maintenance of non-responsiveness to dietary antigens and commensal flora. *Immunol. Rev.* 213: 82–100.
3. Kraehenbuhl, J. P., and M. R. Neutra. 2000. Epithelial M cells: differentiation and function. *Annu. Rev. Cell Dev. Biol.* 16: 301–332.
4. Pabst, O., G. Bernhardt, and R. Forster. 2007. The impact of cell-bound antigen transport on mucosal tolerance induction. *J. Leukocyte Biol.* 82: 795–800.
5. Martinoli, C., A. Chiavelli, and M. Rescigno. 2007. Entry route of *Salmonella typhimurium* directs the type of induced immune response. *Immunity* 27: 975–984.
6. Hashizume, T., A. Togawa, T. Nochi, O. Igarashi, M. N. Kweon, H. Kiyono, and M. Yamamoto. 2008. Peyer's patches are required for intestinal immunoglobulin A responses to *Salmonella*. *Infect. Immun.* 76: 927–934.
7. Macpherson, A. J., and T. Uhr. 2004. Compartmentalization of the mucosal immune responses to commensal intestinal bacteria. *Ann. NY Acad. Sci.* 1029: 36–43.
8. Suzuki, H., S. Sekine, K. Kataoka, D. W. Pascual, M. Maddaloni, R. Kobayashi, K. Fujihashi, H. Kozono, J. R. McGhee, and K. Fujihashi. 2008. Ovalbumin-protein sigma 1 M-cell targeting facilitates oral tolerance with reduction of antigen-specific CD4$^+$ T cells. *Gastroenterology* 135: 917–925.